The role of the Foxo transcription factors in normal and aberrant late lung development

Inaugural Dissertation

submitted to the

Faculty of Medicine

in partial fulfilment of the requirements

for the PhD-Degree

of the Faculties of Veterinary Medicine and Medicine

of the Justus Liebig University Giessen

by Francesco Palumbo

of Taranto, Puglia, Italy

Giessen (2023)

From the Max-Planck-Institute for Heart and Lung Research. Department IV Lung Development

Director: Prof. Dr. Med. Werner Seeger

of the Faculty of Medicine of the Justus-Liebig-Universität Gießen

First Supervisor and Committee Member Prof. Dr. Rory Morty

Second Supervisor and Committee Member Prof. Dr. Wolfgang M. Kuebler

Committee Members Prof. Dr. Jaan Toelen, Prof. Dr. Norbert Weissmann

Date of Doctoral Defense

May 9th 2023

1 Table of contents

2 Introduction

The mammalian lung is composed of a complex network of cells and structures which work synergically to ensure the primary function of the respiratory system: to perform gas exchange. Oxygen is transported from the atmosphere to the bloodstream so that it can reach every tissue while carbon dioxide is directed from the bloodstream to the atmosphere. The functional unit of the respiratory system, the alveolus, relies on two branching networks, epithelial and vascular, to accomplish this function (16, 65). In the alveolar epithelium, several cell types have been accreditated with a pivotal role in facilitating gas exchange. The type 2 pneumocytes (AT2) are known to secrete surfactants and differentiate in type 1 pneumocytes (AT1) upon injury (11, 57). The AT1 cells serve not only as a structural scaffold of the alveolar network, acting as a template for endothelial morphogenesis, but also retain plasticity features as can transdifferentiate into AT2 cells, thus driving alveolar regeneration (31, 68). Along with the epithelial and the endothelial compartments, several other cell types such as airway and vascular smooth muscle cells (36, 44), lipofibroblasts (3) and myofibroblasts (59) have been proposed to play critical roles in supporting the development of the lung, being involved in crucial processes of lung regeneration.

2.1 Lung development in human and mouse

Lung morphogenesis is divided into four distinct stages, which are defined by structural and morphological modifications. This staging method - in the mouse - can be summarized as: pseudoglangular, canalicular, saccular and alveolar stage. In the pseudoglandular stage (human: week 4–17; mouse: embrionic (E) 9.5–E16.5) the branching morphogenesis takes place, the terminal bronchioles are formed and the epithelial progenitors specify in terminally differentiated cell types such as basal, neuroendocrine, ciliated and secretory cells. The canalicular stage (human: week 17–26; mouse: E16.5–E17.5), is characterized by the further branching of the bronchioles and the differentiation of the capillaries. In the saccular stage (human: 26 to 36 weeks of gestation; mouse: E17.5–P5) the alveolar sacs are formed, the mesenchyma is thinned to facilitate the gas exchange and surfactant is produced. In the alveolar stage (human: ~36 weeks to 8 years; mouse: P5–P30) the alveolar sacs differentiate to mature alveoli in the so called process of alvelologenesis (16, 17) This phase is characterized by elastin deposition in the primary septa to give rise to the secondary septa (17). The human lung is already in the alveolar stage at birth, the mouse

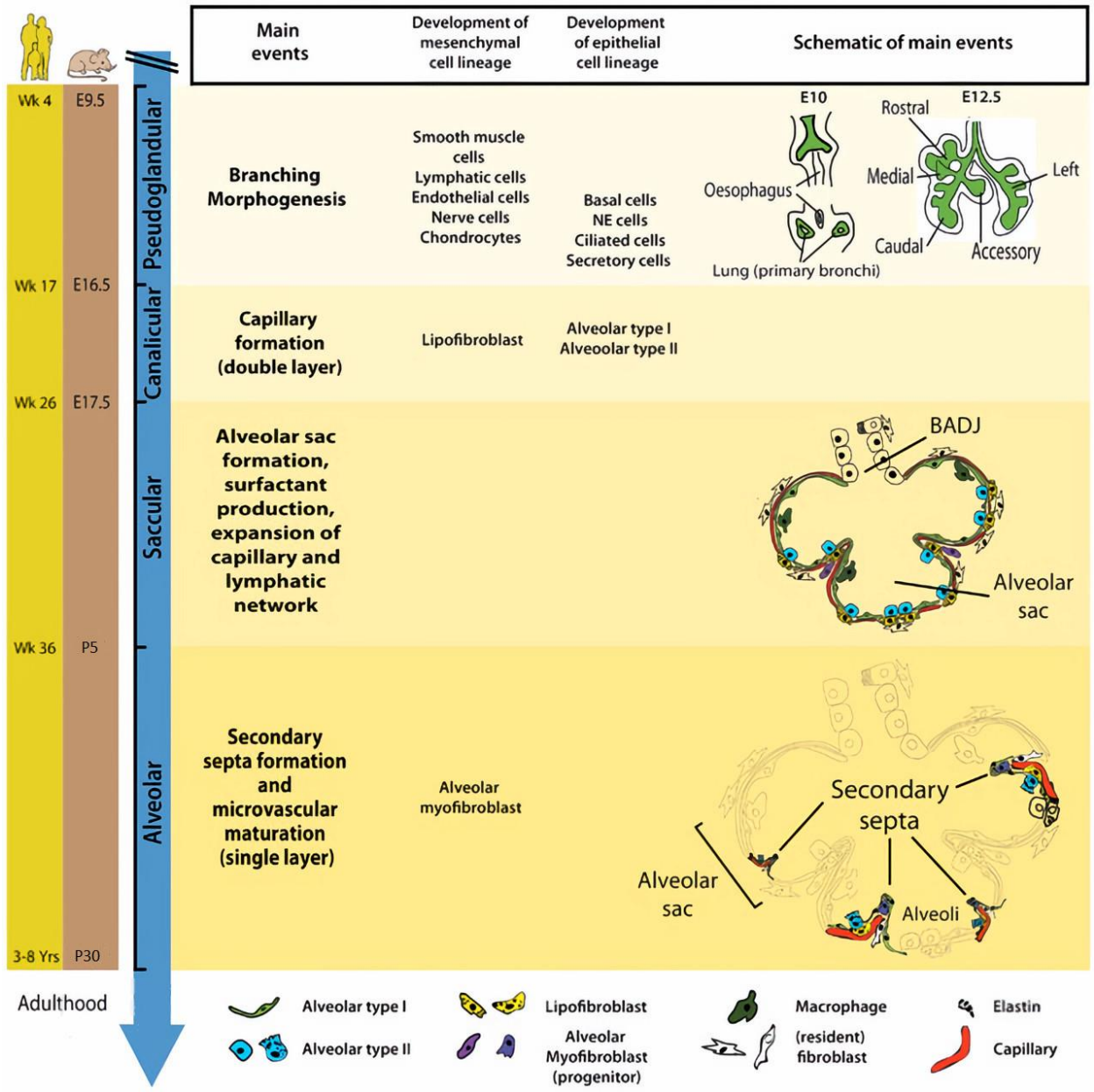

Figure 1 – Schematics of the timeline and stages in lung development of human and mouse. Lung morphogenesis is divided in four different stages: pseudoglandular (human: week 4–17; mouse: E9.5–E16.5), canalicular (human: week 17–26; mouse: E16.5–E17.5), saccular (human: 26 to 36 weeks of gestation, mouse: E17.5–P5) and alveolar (human: ~36 weeks to 8 years; mouse: P5–P30). At birth the human lung is already in the alveolar stage, the mouse is born with the lung in the saccular stage. Newborn mice have functional lungs in the saccular stages at birth. The human lung is still not fully functional in the saccular stages. Therefore, babies born in the saccular stage are considered preterm. This figure was adapted from (11). Wk, week; E, embryonic; P, postnatal; NE, neuroendocrine.

lung is born with the lung in saccular stage. This difference offers a great advantage in the contest of studying the pathogenesis of bronchopulmonary dysplasia (BPD). The mouse lung is born in the saccular stage, which coincides with the human preterm infant, often born in the saccular stage as well. The mouse offers the possibility to expose the lung to O_2 in the same developmental stage a preterm baby would receive O_2 supplementation (12). Several molecular pathways have been reported to play a crucial role in the stages of late lung development. Among them, several transcription factors are included. Homebox protein a5 (Hoxa5) and homebox protein b5 (Hoxb5) have been reported to be important modulators of branching morphogenesis. The deletion of Hoxa5 was found to induce respiratory distress and primary lung defects with partially penetrant lethality at birth (10). Furthermore, the deletion of forkhead box protein j1 (Foxj1) was shown to lead to defects in lung function and abnormal differentiation of the ciliated cells (18, 48). The regulation of glioma associated zinc finger protein 2 (Gli2) is associated with the most severe perturbations in the lung. The absence of the Gli2 transcription factor precludes lung and tracheal development along with that of other organs (45). To date, the role of the forkhead box o (Foxo) transcription factors in the contest of apoptosis-regulated endothelial development and O_2-induced arrested lung development has not been elucidated. This study is the first to report the involvement of the Foxo transcription factors during late lung development and in a mouse model of BPD.

2.2 Bronchopulmonary dysplasia

In 1967, William Northway, employing chest radiography, described for the first time the respiratory function of preterm babies which was significantly compromised similarly to respiratory distress syndrome (RDS), due to hyperinflation, airway abnormalities and parenchymal infiltrates (50). This condition often required O_2 supplementation by mechanical ventilation, leading to severe lung injury and fibrosis. Northway's observations led to characterize the clinical features of a new disease typical of preterm babies, which Northway called bronchopulmonary dysplasia. This report, which is still considered one of the most impactful studies in the field of neonatology, led the attention of the scientific community to find new clinical care strategies to help preterm babies to survive and understand better normal and aberrant lung development in the contest of O_2 supplementation (19, 66). By that time, advances have been made, but many pathomechanisms of BPD are still poorly understood. The employment of surfactants and other strategies of perinatal care led to a new form of BPD with mild or no airway injury, and minimal

fibrosis, but arrested lung development (41). For this reason, BPD is considered a developmental disease characterized by: decreased septation, alveolar hypoplasia, low surface area for gas exchange and dimorphic vascular development. Extremely low gestational age babies (born at 24-28 weeks) are known to be at greater risk of BPD (29). These preterm patients are born during the saccular or the canalicular stage of lung development, in which the juxtaposition of the airways with the pulmonary vessels takes place (70). In addition, due to vascular remodelling, 16-25% of BPD patients develop pulmonary hypertension (PH), which contributes significantly to increased morbidity and mortality (46). Despite tremendous efforts to understand the pathomechanisms of BPD over the past decades, many details in the processes are still poorly understood. The mechanisms governing the response of the endothelium in the pathogenesis of BPD are the most obscure (70). Therefore, elucidating some mechanisms typical of the pathogenesis of BPD which has not been yet clarified, is also the aim of the present study. To date, a limited number of studies address the role of lung microvasculature in BPD. De Paepe and coworkers reported a significant reduction in the expression of the endothelial marker platelet endothelial cell adhesion molecule 1 (Pecam1) on the surface of the endothelial cells of the lungs of babies who received mechanical ventilation and died of BPD. In contrast, imaging analysis revealed increased proliferation in capillaries of BPD lungs compared with age-matched controls. Stereological quantification of the lung microvasculature demonstrated that by increasing the exposure time of ventilation, the vascular volume was significantly increased. Furthermore, the relative area of the endothelial cells was reduced in ventilated patients compared with the controls. These data suggest a characteristic dysmorphism of the lung microvasculature in BPD patients (22). However, comparing data obtained by autopsy specimens can be challenging to interpret and could be not representative of the whole spectrum of a disease as data from such probes represent the most dramatic cases (6).

2.3 Murine model of bronchopulmonary dysplasia

Several experimental models have been developed to study the pathogenesis of BPD. The need to establish which models could better translate the pathogenesis of BPD, recently led to a systematical review of the strengths and limitations of common animal models of BPD (7). The most widely used are the hyperoxia-based mouse and rat models, which were extensively reviewed (12, 51). Along with mouse and rat models, other models have been employed in experimental

BPD, such as the preterm and term rabbit models (20), the chronically ventilated preterm lamb model (4), and the preterm baboon model (81). Each model has advantages and disadvantages. For instance, the greater the size of the animal employed in the model, the more the model is better translationally recognized, as the more the animals are evolutionarily related to the human. On the other hand, the bigger the size of the animal, the more challenging it is to deal with husbandry. Although the use of small animals has technical difficulty due to size, the mouse model has the advantage of broad possibilities in genetic manipulation. As a result of the critical evaluation of the different models of BPD, several questions emerge and several studies have been recently conducted. Nardiello and coworkers extensively evaluated the impact of O_2 concentration in murine experimental BPD, reporting that different strategies of O_2 supplementation yield different outcomes in terms of lung structure perturbations. A mild model of hyperoxia employing 60% O_2 supplementation, was demonstrated more suitable than an 85% O_2 model in evaluating the effects of cotton seed oil as an intervention to ameliorate damaged lung structure (49). These remarkable data clearly demonstrate how there is no standardized method to generate a model of BPD, pointing out the need to choose a strategy to best mimic the pathomechanisms of interest. Along the line of assessing the effectiveness of an intervention, Rath and collaborators demonstrated that caffeine administration was not able to drive lung alveolarization in mice (56). Conversely, monkey, rabbit and rat models of BPD have been shown to be suitable to study the effects of caffeine as a driver of lung regeneration (20, 51, 81). Tiono and coworkers compared the effect of hyperoxia on lung development in different mouse strains. The report highlights similarities and differences among the strains employed, demonstrating that the different genetic backgrounds had an impact on the morphometric and molecular responses of the lung to hyperoxic insult (72). Along with the studies mentioned above, several other issues are waiting to be addressed in the context of modelling BPD. For instance, one of the challenges in the near future is to investigate which model is the most suitable to mimic lung function in BPD. Although the most promising strategy to mimic BPD is hyperoxia, the studies reported above demonstrate the need to consider critically the variety of experimental approaches currently employed in the field to develop and optimize the most suitable approach for each of the several aspects of the pathogenesis of BPD.

2.4 The Foxo transcription factors

The Foxo proteins are a family of evolutionarily conserved transcription factors that are accreditated with a pivotal role in a wide range of molecular and functional processes such as cell cycle regulation, apoptosis, differentiation, and response to metabolic stress (30). Several lines of evidence underscored the involvement of Daf-16 activation in the regulation of the life span processes in *Caenorhabditis elegans* (42). In mammals, the Foxo transcription factor family was first described by Biggs and collaborators (13). In mice and humans, the Foxo transcription factor family is represented by four members: Foxo1, Foxo3, Foxo4, Foxo6. The genes Foxo1, Foxo3 and Foxo4 are known to share the largest homology as well as overlapping downstream transcriptional activities (1). At the functional level, Foxo transcription factors are involved in the regulation of the homeostasis of many organs such as the liver (71), brain (54) and heart (58) as well as in the response of several pathologies such as cancer, diabetes and neurodegenerative diseases (52). Several lines of evidence point to the Foxo transcription factors as key contributors to the regulation of lung homeostasis and response to diseases. A recent study by Savai and coworkers reported that the downregulation of Foxo1 is a key feature of experimental and human PH. The pharmacological activation of Foxo1 with Paclitaxel normalized lung vascular remodelling and right heart hypertrophy *in vivo* (61). Pulmonary hypertension is reported to be often associated with BPD (77). A recent report from Weismann and collaborators has shown that about the 25% of infants with moderate to severe BPD develop BPD-associated PH resulting in increased morbidity and mortality (79). In the line of regulation of vascular remodelling, the Foxo transcription factors have been accreditated as pivotal players in the modulation and development of endothelial cell morphology (43). The global deletion of Foxo1 (but not Foxo3 and Foxo4) is lethal during the embryogenesis at E11 because of abnormal vascular remodelling, thus suggesting the important involvement of Foxo1 in regulating the development of the mouse vasculature (23, 33). A report from Skurk and coworkers pointed out the intimate connection between the activity of the Foxo transcription factors and the regulation of apoptosis in endothelial cells. These researchers induced the overexpression of Foxo3 in human umbilical vein endothelial cells (HUVECs) *in vitro* (67). Enhancing Foxo3 expression resulted in increased apoptosis through the inhibition of the Caspase-8 homolog flice-inhibitory protein (Flip). In addition, the constitutive expression of protein kinase b (Pkb) also known as Akt was shown to induce Foxo3 nuclear exclusion, proposing the Akt pathway as an important regulator of Foxo3 activity in the endothelial

cells (67). In this line, it has been shown that the activation of the phosphoinositide 3-kinase (Pi3k) pathway can inhibit Foxo1 and Foxo3 nuclear exclusion by phosphorylation at T32, S253, and S315 leading to inhibition of the Foxo's DNA binding activity, thus triggering to induction of apoptosis in lung mouse fibroblast (2). The Foxo transcription factors have been also accreditated to be crucial modulators of the endothelial response to growth factors, in a mechanism that is highly regulated by the Akt pathway. For instance, stimulating bovine lung microvascular endothelial cells (BLMVECs) with angiopoietin 1 (Ang1) resulted in Akt phosphorylation at S470 and as consequence phosphorylation of Foxo1 at S256 and T24 (21). In addition, in Foxo1-deficient endothelial cells, stimulation by vascular endothelial growth factor (VEGF) failed to induce the elongation of the endothelial cells compared with the wild-type colonies (43). Furthermore, inhibiting Foxo1 in vascular proliferating endothelial cells (VPCs) resulted in a consistent reduction in the vascular elongation of the cell colonies, which was promoted in wild-type cells treated with the Akt inhibitors LY294002 and VIII (75). One other element of the signal transduction which is reported to be crucial in the regulation of the Foxo signalling is the transforming growth factor β (Tgf-β) signalling pathway. Seoane and coworkers employed chromatin immunoprecipitation to identify the small mother against decapentaplegic 3 and 4 (Smad3 and Smad4) proteins as crucial binding partners of the Foxo proteins upon Tgf-β stimulation. Tgf-β-mediated Foxo1, Foxo3 and Foxo4 transcriptional activation resulted in the upregulation of several downstream genes such as cyclin-dependent kinase inhibitor 1 (p21cip), Intermediate-density lipoprotein 1 (Idl1) and basic helix-loop-helix transcription factor mic (c-myc) (64). Moreover, Tgf-β was reported to induce the elongation of mouse embryo-derived endothelial cells, but not in Foxo1-null cells. In addition, the genetical activation of Foxo1 in a Tet-Foxo-derived cell colony increased the colony elongation in a manner comparable to Tgf-β stimulation (43). Given that the Tgf-β pathway plays a crucial role in the pathogenesis of human and experimental BPD, the transcriptional regulation of the Foxo signalling through Tgf-β is a clear indication of the importance of the Foxo transcription factors in governing processes of normal and aberrant lung development. In addition to Smad3 and Smad4, several other proteins have been proven to play a direct role in the modulation of Foxo transcriptional activity (76). Almeida and coworkers reported that hydrogen peroxide-induced oxidative stress promoted the interaction of Foxo1 as well as Foxo3 with β-catenin, thus inducing the transcription of genes such as Catalase and growth arrest and DNA damage inducible protein 45 (Gadd45)

which are known to be involved in the modulation of osteoblastic development (5). Foxo1 has been also accreditated to govern crucial processes during a primate's pregnancy in association with one other transcription factor known to play a pivotal role in several developmental processes. The gene expression of Foxo1 and homebox protein a10 (Hoxa10) were found to significantly increased during the late stage of the baboon's pregnancy contributing to the activation of the insuling growth factor (Igf) pathway. In fact, Foxo1 was found to directly associate with Hoxa10, thus inducing the insulin growth factor binding protein 1 (Igfbp1) promoter activity in primate endometrial cells (37). To address the genetic signature of the Foxo transcription factors in the endothelial cells, Potente and colleagues employed gene silencing approaches to investigate the role of the Foxo's in the regulation of vascular development *in vitro*. The genetical ablation of Foxo1 by siRNA promoted the downregulation of cyclin dependent kinase inhibitor 1b (Cdkn1b) (55). Whereas the employment of a viral vector overexpressing Foxo1 upregulated Cdkn1b and reduced the proliferating cell nuclear antigen (Pcna) which is known to be activated in response to the DNA damage (8). Furthermore, Ang1 treatment reduced Foxo1 and consequently Cdkn1b expression in HUVECs cells, thus inhibiting endothelial apoptosis (21). These studies, taken together, accredited Cdkn1b as the most conserved target gene of Foxo1 in endothelial cells. Despite several studies addressing the role of the Foxo transcription factors in regulating the endothelial homeostasis and stress response *in vitro*, studies investigating the functions of the Foxo's during normal and aberrant lung endothelial development *in vivo* are still very limited. As well as, no study has been conducted in investigating the role of the Foxo transcription factors in the pathophysiology of BPD.

3 Hypothesis and aim of the study

The Foxo transcription factors are accreditated as important regulators of many molecular pathways governing developmental processes, apoptosis, metabolism, and the pathogenesis of several diseases including cancer (27) and pulmonary hypertension (61). To date, no study addressed the role of the Foxo transcription factors in late lung development as well as in the pathogenesis of BPD. Given that the Foxo transcription factors act as important sensors of the lung homeostasis in other diseases (1) and in the development of the vasculature of the mouse (43), the hypothesis of this study was that the Foxo transcription factors are important modulators of late lung development and play an important role in the pathogenesis of BPD. The aim of this study was to characterize the role of the Foxo transcription factors in the regulation of the lung structure and mechanistics in a mouse model of BPD. Moreover, it is objective of this study to define which molecular pathways are involved in the ability of the Foxo transcription factors to govern late lung development and the response to hyperoxia.

4 Materials and Methods

4.1 Materials

4.1.1 Technical equipment

The technical equipment used in this study is reported in table 1.

Table 1 – Technical equipment

Name, manufacturer and catalogue number of the equipment used for this study are listed in the table below. A double number sign (##) is used when no catalogue number is reported. (Table 1)

Name	**Manufacturer**	**Catalogue number**
Design-Based Stereology		
24ga×0.5" Dispensing Needles	CML SUPPLY, USA	901-24-050
Agar embedding mould	Made in house	##
Agar slicing mould	Made in house	##
Automated Rotary Microtome RM2255	Leica, Germany	CM3050S
Bone Cutting Spring Scissors	FST, Germany	16144-13
Conical tubes. 5 ml	Eppendorf, Germany	30119401
Cotton buds	ROTH, Germany	XL54.J
Delicate Suture Tying Forceps	FST, Germany	11063-07
Digital scale	Kern, Germany	EMB-20002
Digital Slide Scanner	Hamamatsu Photonics, Japan	Nano Zoomer-XR C12000
Extra Fine Graefe Forceps	FST, Germany	11150-10
Fine Scissors	FST, Germany	14058-11
Glass vials, 5ml	ROTH, Germany	LC82.1
HDSLR Nikon D5300Camera	Nikon, Japan	D5300
Histobloc	Morphisto, Germany	11282.VE001
Histological section water bath	Vogel, Germany	VB693
Latex-free multi-way tap system	Braun, Germany	2133076

Table 1 – continued

Name	**Manufacturer**	**Catalogue number**
Microscope slides	Thermo Fisher Scientific, USA	J1800AMNZ
Microtome Knife	Leica, Germany	14021604813
Microwave Oven	Samsung Electronics, Korea	MS28F303T
Oxygen exposure chamber	BioSpherix, USA	##
Polyamide suture thread	SMI, Germany	4015x
Round Handled Suture Tying Forceps	FST, Germany	18026-10
Safety Bench Hood	Thermo Fisher Scientific, USA	3124
Snap-on lid	ROTH, Germany	LC87,1
Spring Scissors	FST, Germany	15006-09
Static O_2 Controller	Bio Spherix, USA	ProOx 110
Syringe, 50 ml	Braun, Germany	8728844F
Technical Graph Paper 1mm scale	Hahnemühle, Germany	10662561
Teflon embedding mould, Histoform	Morphisto, Germany	15068.VE001
Trimming blade No.130R	Feather, Germany	205.500.000
Vannas Spring Scissors - 2.5mm Cutting Edge	FST, Germany	15000-08
Warm plate	Medax, Germany	12895
Western blot		
Criterion Stain-Free Tris-HCl Protein Gel, 26 well, 15 µl	Bio-Rad, USA	3450426
Criterion™ Cell	Bio-Rad, USA	1656001
Digital camera system, ImageQuant™ LAS 4000	Fujifilm Life Science, USA	LAS4000
Mini-PROTEAN® Tetra Cell	Bio-Rad, USA	1658000
Mini-PROTEAN® Tetra Cell Casting Modules	Bio-Rad, USA	1658009

Table 1 – continued

Name	Manufacturer	Catalogue number
PowerPac™ Basic Power Supply	Bio-Rad, USA	1645050
PowerPac™ HC High-Current Power Supply	Bio-Rad, USA	1645052
Precellys 24 tissue homogenizer	Bertin, USA	P000669-PR240-A
Reagent Reservoir	Axygen, USA	RES-V-25-S/
Spectrophotometer, Infinite® 200 PRO	TECAN, Switzerland	800-7499
Thermomixer Compact	Eppendorf, Germany	5350
Trans-Blot Turbo Midi Transfer System	Bio-Rad, USA	1704150
Trans-Blot Turbo Mini Transfer System	Bio-Rad, USA	1704156
Trans-Blot® Turbo™ Transfer System	Bio-Rad, USA	1704150
Cell culture		
Bürker Counting Chambers	Thermo Fisher Scientific, USA	10513451
Cell scraper 25CM 2PO/CS100	Sarstedt Inc, Germany	831.830
Cellstar 6 Well Cell Culture Plate	Greiner, Germany	657160
CO_2 Incubator	Thermo Fisher Scientific, USA	50116047
Filter unit 0.22 µm	Millipore, Ireland	GSWP04700
Integra Biosciences™ Vacusafe™ Comfort Aspiration system	Thermo Fisher Scientific, USA	158310
Inverted Microscope	Leica, Germany	11526201
T 75 Flasks	Greiner, Germany	658175
Wather bath	VWR, USA	VWB 12
Flow Cytometry		
Drilled 50 ml Falcon lid	Made in house	##

Table 1 – continued

Name	Manufacturer	Catalogue number
EASYstranier 100 µm	Greiner bio-one, Germany	542000
EASYstranier 40 µm	Greiner bio-one, Germany	542040
FACS Aria III	Becton Dickinson, USA	##
LSR Fortessa	Becton Dickinson, USA	##
Paraflim	Bemis, USA	PM-999
Screens for CD-1™	Sigma-Aldrich, USA	S4020-5EA
Mouse Genotyping		
Centrifuge MiniSpin®	Eppendorf, Germany	5452000018
Compact Digital Rocking Shaker	Thermo Fisher Scientific, USA	GZ-04725-07
Compact scale	AND Waightning, USA	EK300i
Intas gel IX imager	Instas, USA	Z363820
Mini-PROTEAN® Tetra Vertical Electrophoresis Cell	Bio-Rad, USA	1658004
PowerPac 200 Power Supply	Bio-Rad, USA	BP-200
Quantitative polymerase chain reaction		
NanoDrop One Microvolume UV-Vis Spectrophotometer	Thermo Fisher Scientific, USA	ND-ONE-W
QuantStudio™ 3 Real-Time PCR System	Thermo Fisher Scientific, USA	A28567
General equipment		
Name	**Manifacturer**	**Catalogue number**
Combitips® advanced 0.5 ml	Eppendorf, Germany	30089669

Name	Manufacturer	Catalogue number
Combitips® advanced 10 ml	Eppendorf, Germany	30089677
Combitips® advanced 50 ml	Eppendorf, Germany	30089847
Electronic Pipette 0.5-10 µl	Eppendorf, Germany	2231000777
Electronic Pipette 1-20 µl	Eppendorf, Germany	2231000778
Electronic Pipette 15-300 µl	Eppendorf, Germany	2231000781
Electronic Pipette 50-1000 µl	Eppendorf, Germany	2231000782
Electronic Pipette 5-100 µl	Eppendorf, Germany	2231000779
Heraeus Multifuge 3SR Plus	Thermo Fisher Scientific, USA	75004371
Mechanical Pipette 0.1-2.5 µl	Eppendorf, Germany	3123000012
Mechanical Pipette 0.5-10 µl	Eppendorf, Germany	3123000020
Mechanical Pipette 0.5-5 ml	Eppendorf, Germany	3123000071
Mechanical Pipette 100-1000 µl	Eppendorf, Germany	3123000063
Mechanical Pipette 10-100 µl	Eppendorf, Germany	3123000047
Mechanical Pipette 20-200 µl	Eppendorf, Germany	3123000055
Mechanical Pipette 2-20 µl	Eppendorf, Germany	3123000098
Microcentrifuge	VWR, USA	CT15RE
Microcentrifuge, accuSpin™, Micro 17R	Thermo Fisher Scientific, USA	S39740
Sartorius scale	VWR, USA	vWR-124
Thermocycler, peqSTAR	VWR, USA	732-2773
Vortex mixer	VWR, USA	444-1383
Bulk RNA-seq		
LabChip Gx Touch 24	Perkin Elmer, USA	CLS138162
NextSeq500 instrument	Illumina, USA	SP-104-5506

4.1.2 Reagents

The reagents used in this study are reported in Table 2.

Table 2 – Reagents
Name, manufacturer and catalogue number of the reagents used for this study are listed in the table below. A double number sign (##) is used when no catalogue number is reported. (Table 2)

Name	**Manufacturer**	**Catalogue number**
Design-Based Stereology		
Paraformaldehyde	Sigma-Aldrich, Germany	P6148-500G
4-2-hydroxyethyl-1-piperazineethanesulfonic acid	Sigma-Aldrich, Germany	H0887-100ML
Acetone 99%	ROTH, Germany	T906.1
Agar-Agar	ROTH, Germany	2266.1
Glutaraldehyde 50 % solution in water	Serva, Germany	23116.02
Hydrochloric acid	ROTH, Germany	T134.1
Osmium tetraoxide	ROTH, Germany	8371.1
Phosphate buffered saline	Sigma-Aldrich, Germany	P5493-1L
Sodium cacodylate	Serva, Germany	15540.03
Sodium hydroxide	ROTH, Germany	9356.1
Technovit 3040 powder	Morphisto, Germany	64708806
Technovit 7100	Morphisto, Germany	64709003
Technovit Universal Liquid	Morphisto, Germany	66022678
Uranyl acetate dihidrate	Serva, Germany	77870.01
Western Blot		
Ammonium persulfate	Sigma-Aldrich, Germany	A3678-100G
Anti-Foxo1 antibody	Abcam, USA	ab52857
Anti-Foxo4 antibody	Abcam, USA	ab128908

Table 2 – continued

Name	Manufacturer	Catalogue number
Anti-rabbit antibody	Cell Signaling, USA	7074
Anti-β-actin antibody	Cell Signaling, USA	4967L
Bovine serum albumin	Sigma-Aldrich, Germany	A9418-100G
Clarity Western ECL Substrate	Bio-Rad, USA	1705061
cOmplete™ Inhibitor Cocktail	Sigma-Aldrich, Germany	11697498001
Glycine	ROTH, Germany	0079.2
Loading Buffer	Home made	
phospho-Foxo1 Ser-256	Cell Signaling, USA	9461
Protein Dual Color Standards	Bio-Rad, USA	1610374
Radioimmunoprecipitation assay (RIPA) buffer	Sigma-Aldrich, Germany	R0278-500ML
ROTIPHORESE®Gel 30	ROTH, Germany	3029.1
Sodium dodecil sulfate solution 10%	Promega, Germany	V6551
Sodium orthovanadate	Sigma-Aldrich, Germany	S6508-50G
Tetramethylethylenediamine	Bio-Rad, USA	1610801
Trans-Blot Turbo PVDF	Bio-Rad, USA	1704156
TRIS	ROTH, Germany	9140.3
Cell Culture		
DMEM, low glucose, GlutaMAX	Thermo Fisher Scientific, USA	21885025
Endothelial Cell Growth Medium	Lonza, Switzerland	CC-3162
Fetal Bovine Serum	Thermo Fisher Scientific, USA	A4766801
Ham's F12 Medium	Lonza, Switzerland	BE12-615F
Heparin sodium salt	Thermo Fisher Scientific, USA	H3393-100KU
L-Glutamine	Thermo Fisher Scientific, USA	25030081
Penicillin-Streptomycin	Thermo Fisher Scientific, USA	15070063

Table 2 – continued

Name	Manufacturer	Catalogue number
Endothelial Cell Growth Supplement	Coroning, USA	356006
Flow Cytometry		
Collagenase A	Sigma-Aldrich, Germany	10103586001
APC anti-mouse CD45 Antibody	BioLegend, USA	147708
DAPI dihydrochloride	Sigma-Aldrich, Germany	D9542-10MG
FITC Annexin V Apoptosis Detection Kit	BioLegend, USA	640914
Flow Cytometry Staining Buffer	Thermo Fisher Scientific, USA	00-4222-26
PE anti-mouse CD31 Antibody	BioLegend, USA	102508
Rat Anti-Mouse CD16/CD32	Becton Dickinson, USA	553142
Real-time PCR		
peqGOLD Total RNA Kit	VWR, Germany	12-6834-01
10X PCR Buffer	Thermo Fisher Scientific, USA	N8080006
dNTPs Mix	Promega, USA	U151B
Magnesium chloride, 25 mM	Promega, USA	A351H
Magnesium chloride, 50 mM	Thermo Fisher Scientific, USA	Y02016
M-MLV Reverse Transcriptase (200 U/µL)	Thermo Fisher Scientific, USA	28025021
Nuclease-Free Water	Thermo Fisher Scientific, USA	1388315
Platinum™ SYBR™ Green qPCR SuperMix-UDG	Thermo Fisher Scientific, USA	11733-46
Random Hexamers, 50 µM	Thermo Fisher Scientific, USA	N8080127
RNase Inhibitor	Thermo Fisher Scientific, USA	N8080119
RNase-Free DNase Set	Qiagen, Germany	79254
RNeasy Micro Kit	Qiagen, Germany	74004

Table 2 – continued

Name	Manufacturer	Catalogue number
Mouse genotyping		
5× Colorless GoTaq® Flexi Buffer	Promega, USA	M890A
Magnesium Chloride, 25 mM	Promega, USA	A351B
Quick-Load® Purple 50 bp DNA Ladder	New England BioLabs, USA	N05565
TAE Buffer	ROTH, Germany	0122.1
Bulk RNA-seq		
DNase-FreeDNase Set	Qiagen, USA	79254
RNeasy Plus micro kit	Qiagen, USA	74034
SMART®-SeqHT kit	Takara Clontech, Japan	634455

4.1.3 Software

The software used in this study are listed in the table below (Table 3).

Table 3 - Software

Name	Company, location
Adobe Illustrator	Adobe, USA
Camera Control Pro 2	Nikon, Japan
FlowJo	FlowJo LLC, USA
GraphPad Prism 7.0	GraphPad, USA
ImageJ	NIH, USA
ImageQuant LAS 4000	GE Healthcare, United Kingdom
InstasGelCaptureEntry	Intas, India

Table 3 - continued

NDP.view2	Hamamatsu, Japan
Quant Studio Software	Thermo Fisher Scientific, USA
Visiopharm newCAST	Visiopharm, Denmark
Microsoft Office	Microsoft, Usa
NDP.scan	Hamamatsu, Japan

4.2 Methods

4.2.1 Hyperoxia-based model of bronchopulmonary dysplasia

Newborn mouse pups were randomized to equal litter size for each nursing dam. The cages were placed in an O_2 chamber to be exposed to either normoxia (21% O_2) or hyperoxia (85% O_2) within the first four hours of birth from postnatal day 1 (P1) to postnatal day 14 (P14) (49) (approvals B2/344, B2/1051, and B2/2046). The concentration of O_2 was maintained constant during the entire time of the experiment and was controlled by an automated sensor which was monitored daily. The mice were exposed to a 12:12 hours dark/light cycle and food and water were provided *ad libitum*. To reduce the toxicity induced by O_2 exposure, each nursing dam was rotated between the normoxia and hyperoxia conditions with an interval of 24 h. Newborn mice were then collected on the fifth, tenth, and fourteenth day of life. The mice were sacrificed by an overdose of pentobarbital via intraperitoneal (IP) injection followed by cervical dislocation, accordingly to the guidelines of the federation of european laboratory animal science association (FELASA).

4.2.2 C57BL/6J wild-type mice

C57BL/6J wild-type mice were purchased from Janvier Labs, France.

4.2.3 Nab-Paclitaxel administration

Newborn mouse wild-type pups were randomized and equally distributed for each nursing dam. 10 µg/g of Nab-Paclitaxel was intraperitoneally administered on postnatal day 5 (P5) and postnatal day 10 (P10). The animals were exposed to 21% or 85% O_2 and sacrificed on P14.

4.2.4 C57BL/6-Gt(ROSA)26Sor$^{tm1(CAG-Foxo1,GFP)Moli}$/J mice

The C57BL/6-Gt(ROSA)26Sor$^{tm1(CAG-Foxo1,GFP)Moli}$/J mice were a kind gift of Dr Ming Li from the Memorial Sloan-Kettering Cancer Center, New York, USA. The mouse line was previously reported to be viable and fertile in both heterozygous and homozygous mice (53). This strain was designed to generate a Foxo1^{AAA} knock-in mice with Cre-recombinase tamoxifen-inducible expression of an HA-tagged human Foxo1 mutant cDNA from the Gt(ROSA)26Sor locus. The targeting vector carries the substitution of alanine on the Akt phosphorylation sites, resulting in a defective nuclear export of the protein. When the mutant mice are bred with a mouse line expressing Cre recombinase, the resulting offspring will express Foxo1 in the targeting tissues upon tamoxifen administration.

4.2.5 Foxo1$^{tm1.1Mrc}$ mice

The Foxo1$^{tm1.1Mrc}$ mice were a generous gift of Prof. Mario Capecchi from the University of Utah School of Medicine, Salt Lake City, USA. This strain was designed to induce the inactivation of the Foxo1 allele by the excision of exon2 and 3 upon tamoxifen-induced Cre recombinase activation (35). When mice belonging to this line are bred to mice expressing Cre recombinase, in the resulting offspring Foxo1 expression is downregulated upon tamoxifen administration.

4.2.6 Tg(Tek-icre/ERT2)1Soff mice

The Tg(Tek-icre/ERT2)1Soff line was a kind gift of Prof. Stefan Offermanns from the Max Plank Institute for Heart and Lung Research of Bad Nauheim, Germany. The mouse line was generated to express Cre- recombinase upon administration of tamoxifen. The targeting vector of these mutant mice was designed to insert a tamoxifen-inducible Cre recombinase gene and an FRT-flanked beta-lactamase gene into the ATG start site of the mouse endothelial tyrosine kinase (Tek) gene. The resulting line was proven to express the Cre recombinase in the endothelial cells of several mouse organs (39).

4.2.7 Gt(ROSA)26Sor$^{tm4(ACTB-tdTomato,-EGFP)Luo}$ mice

The Gt(ROSA)26Sor$^{tm4(ACTB-tdTomato,-EGFP)Luo}$ mice were purchased by The Jackson Laboratory (Stock No. 007676). This mouse strain was designed to contain a single copy of the transgene integrated into the ROSA26 locus. The target vector presents a chimeric CMV-beta-actin promoter, a membrane-targeted tandem dimer Tomato (mT) followed by a polyadenylation signal (pA) flanked by two LoxP sites and a membrane-targeted green fluorescent protein (mG) followed as well by a polyadenylation signal. In absence of tamoxifen stimulation, the construct constitutively expresses the mT gene. Upon tamoxifen administration, the Cre-mediated mT excision induces the expression of the mG gene (47).

4.2.8 Generation of the mouse transgenic lines

The C57BL/6-Gt(ROSA)26Sor$^{tm1(CAG-FOXO1,GFP)Moli}$/J mice were crossed with endothelial specific driver Tg(Tek-icre/ERT2)1Soff to generate a strain of homozygous mice to induce the expression of Foxo1 upon tamoxifen administration (designated strain Tie2-Cre Foxo1^{oe}). To induce the expression of Foxo1, newborn pups were injected intraperitoneally (IP) on P1 and postnatal day 2 (P2) with 0.1 mg/kg of tamoxifen per mouse. To generate a mouse strain that downregulates

expression of Foxo1, Foxo1$^{tm1.1Mrc}$ mice were crossed with Tg(Tek-icre/ERT2)1Soff mice until homozygous mice were obtained (designated strain Tie2-Cre Foxo1^{ff}). Newborn mice from the resulting offspring were injected IP with 0.05 mg/kg of tamoxifen per mouse on P1 and P2. To monitor the efficiency of the Tek-icre/ERT2 transgene, the Tg(Tek-icre/ERT2)1Soff mice were crossed with members of the Gt(ROSA)26Sor$^{tm4(ACTB-tdTomato,-EGFP)Luo}$ mouse line. Newborn pups homozygous for the mTmG transgene were injected IP with tamoxifen on P1 and P2.

4.2.9 Total RNA isolation

Mouse lung biopsies were homogenized using Precellys tubes (Precellys, Bertin, USA, # P000912 LYSK0-A) and Precellys 24- dual homogenizer (Precellys 24 tissue homogenizer, Bertin, USA, P000669-PR240-A). Total RNA was isolated using peqGOLD Total RNA Kit (peqGOLD Total RNA Kit,VWR, Germany, 12-6834-01) accordingly to the manufacturer's instructions. Lung microvascular endothelial cells (LMECs) were centrifuged at 15000 rpm for 15 min at 4 C and total RNA was purified using RNeasy Micro Kit (RNeasy Micro Kit, Quiagen, Germany, #74004) accordingly to the manufacturer's indications.

4.2.10 Gene expression quantification

The concentration of total RNA was measured using NanoDrop One. 1000 ng/ul of total RNA was used to perform the reaction of retrotranscription to convert RNA to cDNA prior 10 min denaturation at 70 ºC in a peqSTAR Thermocycler (VWR, Germany, 732-2886). The retrotranscription was performed by adding 20 µl of master mix from Table 4. The samples were then incubated in a peqSTAR Thermocycler following the protocol in Table 5.

Table 4 - Reagents used for the retrotranscription reaction

Reagent	Volume in µl for one reaction
Nuclease-free water	2.5
10× PCR buffer	4
Magnesium chloride 25 mM	8
Random hexamers	2

Table 4 – continued

Reverse transcriptase	0.5
RNAse inhibitors	1
Total	18

Table 5 – Steps used for the retrotranscription

Reaction	Temperature	Time
Incubation	21 ºC	10 min
Extension	43 ºC	75 min
Enzyme inactivation	95 ºC	5 min
Storage	4 ºC	long-term

Following the reaction, the cDNA was diluted in 60 µl of nuclease-free water. The real-time PCR reaction was performed using Platinum™ SYBR™ Green qPCR SuperMix-UDG (Thermo Fisher Scientific, USA, 11733046). The reaction was performed by adding 2 µl of cDNA to 23 µl of master mix prepared accordingly to Table 6. The samples were incubated in a QuantStudio™ 3 Real-Time PCR System using the protocol listed in Table 7. The real-time PCR reaction was performed according to the protocol listed in Table 8. DeltaCt values were calculated using the formula mean CT(reference gene) – mean CT(gene of interest).

Table 6 – Reagents used for the real-time PCR reaction

Reagent	Volume in µl for one reaction
Nuclease-free water	2.5

Table 6 - continued

10× PCR Buffer	4
Magnesium chloride 25 mM	8
Random hexamers	2
Total	16.5

Table 7 – Reagents used for the real-time PCR master mix

Reagent	Volume in µl for one reaction
SYBR Green	13
Magnesium Chloride	1
Primer dilution	1
Nucease-free water	8
Total	23

Table 8 – Protocol for the real-time PCR reaction

Reaction	Temperature		Time
Denaturation 1	50 ºC		2 min
Denaturation 2	95 ºC		5 min
Denaturation	40×	95 ºC	0.5 min
Annealing		59 ºC	0.5 min
Extension		72 ºC	0.3 min

Table 8 - continued

Melting Curve 1	95 ºC	0.15 min
Melting Curve 2	60 ºC	1 min
Dissociation	95 ºC	0.15 min
Storage	60 ºC	0.15 min

The primers used in the real-time PCR reaction were diluted 1:10. The sequences of each primer pair used in this study are listed in Table 9.

Table 9 – List of primers for real-time PCR

Gene	Forward (5'-3')	Reverse (5'-3')
Ccne1	GTGGCTCCGACCTTTCAGTC	CACAGTCTTGTCAATCTTGGCA
Cdkn1a	TCAAACGTGAGAGTGTCTAACG	CCGGGCCGAAGAGATTTCGT
E2f1	GCCTGGAGCAAGAAGCAGTA	GTGGGGAGAGGCTGATGAAC
Foxo1	ATGCTCAATCCAGAGGGAGG	ACTCGCAGGCCACTTAGAAAA
Foxo3	GCAAGCCGTGTACTGTGGA	CGGGAGCGCGATGTTATCC
Foxo4	CTTCCTCGACCACCAGACCTCG	ACAGGTCGGTTCGGAGTGT
Foxo6	GTGGGGGAACCTTTCCTACG	TTCTGCACGCGGATGAACC
Polr2a	CTAAGGGGCAGCCAAAGAAAC	CCATTCAGCATACAACTCTAGGC

4.2.11 Protein isolation

Total protein isolation was performed using a lysis solution containing radioimmunoprecipitation assay (RIPA) buffer with 1 mM cOmplete™ Protease Inhibitor Cocktail and 200 mM Sodium orthovanadate as phosphatase inhibitor component. Random autopsies from the right lung of the mice were placed in Precellys tubes (Precellys, Bertin, USA, # P000912-LYSK0-A) and homogenized using a 24-Dual Precellys homogenizer (Precellys 24 tissue homogenizer, Bertin, USA, P000669-PR240-A). The lung homogenate was transferred into 1.5 ml tubes. After 60 min incubation on ice, the sample was centrifuged 30 min at 4ºC with a speed of 14,000 rpm. After centrifugation, the supernatant was transferred to a new 1,5 ml tube. LMVECs were plated at a concentration of 2×10^5 cells/well in a six-well plate. The cells were then harvested, centrifuged 30 min at 4ºC with a speed of 14,000 rpm and the supernatant was replaced with Lysis solution pipetting vigorously. After 60 min incubation on ice, the sample was centrifuged 30 min at 4ºC with a speed of 14,000 rpm and the supernatant was placed in a new 1.5 ml tube. To measure the protein concentration, the protein extracted from the lung homogenate, as well as the Lysis solution, were diluted 1:50 with phosphate-buffered saline (PBS) while the protein isolated from cultured cells or the Lysis solution used for the extraction, were diluted 1:10 in PBS. To generate a curve of standards, bovine serum albumin was diluted in PBS with the following concentrations: 0.05 µg/µl, 0.1 µg/µl, 0.2 µg/µl, 0.3 µg/µl, 0.4 µg/µl, 0.5 µg/µl. Samples and control probes were diluted in 200 µl of Quick Start™ Bradford 1× Dye Reagent (Bio-Rad, USA, #5000205) at a concentration of 5%. The protein concentration was measured with a TECAN spectrophotometer (Tecan, Germany, #Infinite 200 Pro). The average of three independent measurements was used to calculate the volume of protein to load onto each well of the gel.

4.2.12 Polyacrylamide gel electrophoresis

A total amount of 35 µg of protein was diluted with loading buffer solution prepared according to Table 10. After denaturation at 95 ºC for 10 min, the samples were centrifuged at 13,000 rpm for 1 min at RT and loaded onto a home-cast 10% gel accordingly with the protocol listed in Table 11. The proteins were resolved by applying to the gel an electric field using a PowerPac™ Basic Power Supply (Bio-Rad, USA, #1645050) which was run for 1.5 h at 80 V in Running Buffer prepared to dilute 1:5 Tris125 mM-Glycin 1.25M solution in distilled water and adding 0.001% sodium dodecyl sulfate (SDS).

Table 10 – Protocol for preparing Loading Buffer 3×

Reagent	Amount
Distilled water	60 ml
Tris	15 g
Glycerol	15 g
Bromophenol Blue	0.15 g
β-mercaptoethanol	7.5 ml
Sodium dodecyl sulfate	3 g

Table 11 – Protocol for 10% gel preparation

Reagent	Amount	
	SDS-stacking gel	SDS-resolving gel
Acrylamide	5%	10%
Tris 1.5 M pH 8.8	125 mM	375 mM
SDS	0.05%	0.05%
APS	0.05%	0.05%
TEMED	0.065%	0.065%

4.2.13 Western Blot

Separated proteins were transferred to a polyvinylidene difluoride (PVDF) membrane using Trans-Blot Turbo PVDF Transfer Packs (Bio-Rad, USA, #1704156). The transfer was performed using Trans-Blot® Turbo™ Transfer System (Bio-Rad, USA, #1704150). After the transfer, the membrane was washed in gentle shaking for 5 min in PBS-Tween 0.1%. To reduce the non-specific binding of the primary and secondary antibodies, the membrane was incubated in BSA 5% in PBS-Tween 0.1% for one hour at RT. Before washing three times in PBS-Tween 0.1% for 10 min, the membrane was incubated overnight at 4 ºC with the primary antibody. After washing three times in PBS-Tween 0.1% for 10 min, the secondary antibody was incubated for one hour. The membrane was developed using Clarity Western ECL Substrate (Bio-Rad, USA, #1705061) in a Las4000 Digital camera system (Fujifilm, Japan, #LAS4000). The antibodies used to perform protein quantification in this study are listed in Table 12.

Table 12 – List of the antibodies used for western blot

Gene	Manufacturer	Catalogue number
Foxo1	Abcam	ab52857
pFoxo1 S256	Cell Signaling	9461
Foxo4	Abcam	Ab128908
β-actin	Cell Signaling	7074
anti-rabbit	Cell Signaling	4967L

4.2.14 Design-based stereology

The assessment of the lung structure was performed according to the guidelines of the American Thoracic Society and the European Respiratory Society (34). Newborn mice pups were sacrificed at P14. The lungs were instilled through a G24 blunt needle (CML SUPPLY, USA, #901-24-050) via intratracheal cannulation with a fixative solution, under constant hydrostatic pressure of 20 cmH_2O. The fixative was composed of 1.5% (w/v) paraformaldehyde (PFA) (Sigma-Aldrich,

Germany, 158127-500G), 1.5% glutaraldehyde 50% (w/v) (Serva, Germany, 23114.02), 150 mM 4-(2-hydroxyethyl)-1-piperazineethanesulfonic acid (HEPES) solution (Sigma-Aldrich, Germany, 54457) dissolved in 1×PBS, pH 7.4. The trachea was occluded through a surgical wire and incubated in a fixative for 24 h at 4 ºC. The next day, the lungs were dried from the excess of PFA and the trachea, oesophagus and heart were removed before lung volume calculation through Cavalieri´s principle (62). The lungs were embedded in 2% agar dissolved in distilled water and stored at 4 ºC in plastic moulds overnight. The agar block was sliced into 3 mm sections and pictures of each slice were taken with a Nikon D5300 Camera (Nikon, Japan #D5300). The lungs were placed in a 3 ml glass jar. Before washing 4 × 5 min in 0.1 M cacodylate trihydrate, the lung pieces were incubated in 1% osmium tetroxide for 2 h. The lungs were then washed in distilled water for 4 × 15 min and incubated overnight in 2.5% uranyl acetate. After washing 4 × 15 min with distilled water, the lungs were dehydrated 2 × 1h in 70% acetone, 2 × 1 h 90% acetone and 2× 1 h 99.9% acetone. The lung pieces were then incubated overnight in a solution containing 1:1 99.9% acetone: glycol methacrylate and Hardener 1 (Technovit). The solution was removed and the lungs were incubated overnight with pure Technovit. After removing Technovit, the lung pieces were placed in embedding moulds (Morphisto) and infiltrated with a solution made by Technovit, Hardener 1 and Hardener 2. After 48 h the plastic blocks were cast with catting supports using Technovit 7100 dissolved 1:1 with Technovit universal liquid. The blocks were then sliced in 2 µm slices with a microtome (Leica, Germany, RM2255) using a knife (Leica, Germany, #14021608292). For each block of 4 sections, the sections were mounted on glass and stained with Richardson staining solution diluted 1:1 with distilled water. The quantification of the parameters defining the lung structure was estimated as previously described by our group (25, 49, 72). The analysis was assessed using Visiopharm's newCAST™ software.

4.2.15 Flow cytometry

The lungs of newborn mice exposed to 21% or 85% O_2 were used for flow cytometry analysis and fluorescent-activated cell sorting. Each lung was minced and incubated with a digestion solution containing 0.01% Collagenase A (Sigma Aldrich, Germany, #10103586001) in Roswell park memorial institute (RPMI) media (Gibco, Germany, #21875034) in gentle agitation for 10 min at 37 ºC. After filtering with a 150 µm, 100 µm and 40 µm filter, the samples were centrifuged at 13,000 rpm for 5 min at 4 ºC. The single-cell suspension was washed with endothelial cell isolation

media prepared according to Table 13. After resuspending the sample in fluorescent-activated cell sorting (FACS) buffer (BD Bioscience, USA, # 554656), the cells were stained with fluorophore-conjugated antibodies for 20 min in gentle agitation at 4 ºC. The identification of a pure population of lung endothelial cells was performed using CD31 as an endothelial-specific marker and CD45 as an exclusion marker for the immune cell population expressing also CD31. Immediately before the analysis was added 4′,6-diamidino-2-phenylindole (DAPI) to discriminate between live and dead cells.

Table 13 – Reagents for endothelial isolation media

Reagent	Amount
Ham's F12 Medium	40%
DMEM, low glucose, GlutaMAX	40%
Fetal Bovine Serum	20%
L-Glutamine	2%
Penicillin-Streptomycin	1%
Heparin sodium salt	90 mg/l
Endothelial Cell Growth Supplement (ECGS)	100 mg/l

The assessment of early apoptotic lung endothelial cells was performed using FITC-conjugated Annexin V detection kit (BioLegend, USA, 640906) according to the manufacturer´s guidelines. The antibodies used in this study are listed in Table 14. The single-cell suspension was then centrifuged at 13,000 rpm for 5 min at 4 ºC, resuspended in endothelial cell isolation media and

maintained on ice before the analysis.

Table 14 – Antibody used for flow cytometry analysis

Gene	Manufacturer	Catalogue number
PE anti-mouse CD31 antibody	BioLegend, USA	102508
APC anti-mouse CD45 antibody	BioLegend, USA	147708
FITC anti-mouse Annexin V antibody	BioLegend, USA	640914

4.2.16 Pulmonary fibroblast isolation

Pulmonary fibroblasts (PFBs) were isolated by mincing the lung of 11 weeks old C57BL/6J mice and incubating the tissue for 45 min at 37 ºC in 4% Collagenase dissolved in Hank's balanced salt solution (HBSS) with gentle shaking. Before filtration with a 70 µm sieve, the cell suspension was centrifuged for 8 min at 4 ºC at 800 rpm, the supernatant was discarded and the pellet was resuspended in 13 ml of Dulbecco's modified eagle medium (DMEM) Glutamax (Thermo Fisher, Germany, #10566016) with fetal bovine serum (FCS) 10% (Gibco, USA, #26140079) and 1% sodium pyruvate (Thermo Fisher, Germany, #11360070). The cell suspension was then transferred in a T-75 flask and the media was changed every 48 h. After 72 h the cells were detached with trypsin (Thermo Fisher, Germany, #25300054) and seeded 1:3. The cells were used between passages 3 and 6. For each independent experiment, were plated 1×10^5 cells/well in a six-well plate and harvested after 24 h.

4.2.17 Lung microvascular endothelial cells

Mouse lung microvascular endothelial cells (LMECs) were purchased from Creative Bioarray, USA and cultured in SuperCult® Complete Mouse Endothelial Cell Culture Medium (Creative Bioarray, USA, # CSC-C1746). For each independent experiment, were plated 1×10^5 cells/well in a six-well plate. After 24 h the media was removed, the cells were washed with 1×PBS and harvested.

4.2.18 Lung epithelial cell isolation

Lung epithelial cells were isolated from the lungs of 11 weeks old C57BL/6J mice. The lung was perfused with 1×PBS and instilled with Dispase (Corning, USA, # 354235). After 45 min incubation, the lung was minced in a solution containing DMEM, 25% HEPES and 0.6% DNase (Serva, Germany, 9003-98-9) and left in gentle shaking incubation for 10 min. The tissue was then filtered through a 40 µm and 20 µm filter, centrifuged for 8 min at 4 ºC 800 rpm and resuspended in 5 ml of DMEM media. To exclude unwanted cell types, the cell suspension was stained with CD45, CD16/32 and CD31 magnetic beads-conjugated antibodies and incubated for 30 min at 37 ºC. To perform the negative selection of the lung epithelial cells, the cell suspension was placed in a magnet (Invitrogen) which retained the targeted cells. The suspension resulted in a pure population of epithelial cells which were centrifuged and 8×10^4 cells/well were plated onto a

Transwell® Permeable Support (Corning, USA, CLS3464-48EA) in 500 µl of DMEM with 10% FCS and 0.01% Penicillin/Streptomycin and harvested after 24 h.

4.2.19 Pulmonary artery smooth muscle cell isolation

Pulmonary artery smooth muscle cells (PASMCs) were isolated from the pulmonary artery of 11 weeks old wild type mice. After euthanizing and dissecting the mice, the lungs were flushed with 1× PBS. A solution containing 1 mg/ml Collagenase and 10 mg/ml Elastase in 1×HBSS was instilled through the trachea and left for incubation for 25 min at 37 ºC in gentle agitation. The tissue was minced and filtered through a 70 µm. Before centrifugation at 1200 rpm for 5 min at 4 ºC. The supernatant was removed and the pellet was washed with smooth muscle cell growth basal medium (SMGBM) with 10% FBS. The cells were then centrifuged again and resuspended in SMGBM media with 20% FBS and 0.01% penicillin/streptomycin in a 0.75% gelatin-coated T25 flask. The cells were used between passages 3 and 6. For experiments were plated 1×10^5 cells/well in a six-well plate.

4.2.20 Sex genotyping

Tail biopsies were collected from C57BL/6J mice. The total DNA was isolated using Extracta DNA Prep for PCR (Quantabio, USA) according to the manufacturer´s recommendations. Before incubation at 95 ºC for 30 min in 50 µl of Extraction Reagent, the tissue was treated with 50 µl of Stabilization Buffer and used immediately or stored at 4 ºC. The amplification of DNA was performed by PCR. The amplicons were resolved in 1.5% agarose gel by Northern blot. The reagents used for the reaction are listed in Table 15. The amplification protocol used for the PCR reaction is listed in Table 16. The primers used are listed in Table 17.

Table 15 – Reagents used in the PCR reaction for sex genotyping

Reagent	Amount for one reaction
Nuclease free water	31.5 µl
5× PCR Buffer	10 µl

Table 15 - continued

dNTPs	1 µl
Primer dilution 1:10 IL-3	0.6 µl
Primer dilution 1:10 SRY	1 µl
Magnesium chloride	4 µl
Hot start polymerase	0.25 µl

Table 16 - Protocol used for the PCR reaction for sex genotyping

Reaction	Temperature		Time
Denaturation 1	110 ºC		2 min
Denaturation 2	95 ºC		45 min
Denaturation	33×	95 ºC	35 s
Annealing		50 ºC	1 min
Extension		72 ºC	1 min
Dissociation	72 ºC		5 min
Storage	4 ºC		Long term

Table 17 – Primers used for sex genotyping

Gene	Forward (5ˈ- 3ˈ)	Reverse (5ˈ- 3ˈ)
IL-3	GGGACTCCAAGCTTCAATCA	TGGAGGAGGAAGAAAAGCAA
SRY	TGGGACTGGTGACAATTGTC	GAGTACAGGTGTGCAGCAGCTCT

4.2.21 Genotyping for C57BL/6-Gt(ROSA)26Sor$^{tm1(CAG-Foxo1,GFP)Moli}$/J mice

The total DNA of tails from C57BL/6-Gt(ROSA)26Sor$^{tm1(CAG-Foxo1,GFP)Moli}$/J mice was isolated using Extracta DNA Prep for PCR (Quantabio, USA, # 95091-025) according to the manufacturer´s recommendations. Before incubation at 95 ºC for 30 min in 50 µl of Extraction Reagent, the tissue was treated with 50 µl of Stabilization Reagent and used immediately or stored at -20 ºC. The DNA amplification was performed by PCR. The amplicons were resolved in 1.5% agarose gel by Northern blot. The reagents used for the reaction are listed in Table 18. The amplification protocol used for the PCR reaction is listed in Table 19. The primers used for the PCR reaction are listed in Table 20.

Table 18 – Reagents used for the PCR reaction: C57BL/6-Gt(ROSA)26Sor$^{tm1(CAG-Foxo1,GFP)Moli}$/J mice

Reagent	Amount for one reaction
Nuclease free water	28.35 µl
5× PCR buffer	10 µl
dNTPs	1 µl
Primer dilution 1:10	3 µl
Magnesium chloride	5.95 µl
Hot start polymerase	0.25 µl
Total	48.55 µl

Table 19 - Protocol used for the PCR reaction: C57BL/6-Gt(ROSA)26Sor$^{tm1(CAG-Foxo1,GFP)Moli}$/J mice

Reaction	Temperature		Time
Denaturation 1	94 ºC		4 min
Denaturation	34×	95 ºC	35 s
Annealing		65 ºC	45 s
Extension		72 ºC	1 min
Dissociation	72 ºC		5 min
Storage	4 ºC		Long term

Table – 20 Primers used for the PCR reaction: C57BL/6-Gt(ROSA)26Sor$^{tm1(CAG-Foxo1,GFP)Moli}$/J mice

Name	Sequence (5ˈ- 3ˈ)
Wild type forward	GGAGCGGGAGAAATGGATATG
Common reverse	AAAGTCGCTCTGAGTTGTTAT
Mutant forward	AAGACCGCGAAGAGTTTGTC

4.2.22 Genotyping for Foxo1$^{tm1.1Mrc}$ mice

The total DNA from the tails of Foxo1$^{tm1.1Mrc}$ mice was isolated using Extracta DNA Prep for PCR (Quantabio, USA) according to the manufacturer´s recommendations. Before incubation at 95 ºC for 30 min in 50 µl of Extraction Reagent, the tissue was treated with 50 µl of Stabilization Buffer and used immediately or stored at 4 ºC. The amplification of DNA was performed by PCR as previously described (61). The amplicons were resolved in 2% agarose gel by Northern blot. The

reagents used for the reaction are listed in Table 21. The amplification protocol used for the PCR reaction is listed in Table 20. The primers used are listed in Table 22.

Table 21 - Protocol used for the PCR reaction: Foxo1$^{tm1.1Mrc}$mice

Reaction	Temperature		Time
Denaturation 1	95 ºC		5 min
Denaturation	35×	95 ºC	30 s
Annealing		64 ºC	20 s
Extension		72 ºC	1 min
Dissociation	72 ºC		7 min
Storage	4 ºC		Long term

Table 22 – Primers used for the PCR reaction: Foxo1$^{tm1.1Mrc}$mice

Name	Sequence (5'- 3')
CK30 wildtype forward	GTGTACAAACCAGCTGAGCAC
CK142 common reverse	CCTTCAGAGCTGCCAGGTGAATATG
CK143 mutant forward	TGTAGAGAGTATGCCGTCAGAGTGG

4.2.23 Genotyping for Tg(Tek-icre/ERT2)1Soff mice

The total DNA of tails from Tg(Tek-icre/ERT2)1Soff mice was isolated using Extracta DNA Prep for PCR (Quantabio, USA) according to the manufacturer´s recommendations. Prior incubation at 95 ºC for 30 min in 50 µl of Extractio Reagent, the tissue was treated with 50 µl of Stabilization Buffer and used immediately or stored at 4 ºC. The amplification of DNA was performed by PCR as previously described (61). The amplicons were resolved in 1.5% agarose gel by Northern blot.

The reagents used for the reaction are listed in Table 20. The amplification protocol used for the PCR reaction is listed in Table 23. The primers used are listed in Table 24. The primers used for the reaction are listed in Table 25

Table 23 – Reagents used for the PCR reaction: Tg(Tek-icre/ERT2)1Soff mice

Reagent	Amount for one reaction
Nuclease free water	38.1 µl
10×PCR buffer	5 µl
dNTPs	0.4 µl
Primer dilution 1:10	3 µl
Magnesium chloride	2.5 µl
Hot start polymerase	1 µl
Total	50 µl

Table 24 – Protocol used for the PCR reaction: Tg(Tek-icre/ERT2)1Soff mice

Reaction	Temperature		Time
Denaturation 1	94 ºC		4 min
Denaturation	33×	94 ºC	30 s
Annealing		58 ºC	30 s
Extension		72 ºC	45 s

Table 24 - continued

Dissociation	72 ºC	5 min
Storage	4 ºC	Long term

Table 25 – Primers used for the PCR reaction: Tg(Tek-icre/ERT2)1Soff mice

Name	Sequence (5ˈ- 3ˈ)
Wildtype forward	GAAGTCGCAAAGTTGTGAGTTG
Common reverse	TGGCTTGCAGGTACAGGA
Mutant forward	GAGAATGGCGAGAAGTCACTG

4.2.24 Genotyping for Gt(ROSA)26Sor$^{tm4(ACTB-tdTomato,-EGFP)Luo}$ mice

The total DNA of tails from Gt(ROSA)26Sor$^{tm4(ACTB-tdTomato,-EGFP)Luo}$ mice was isolated using Extracta DNA Prep for PCR (Quantabio, USA) according to the manufacturer´s recommendations. Prior to incubation at 95 ºC for 30 min in 50 µl of Extraction Reagent, the tissue was treated with 50 µl of Stabilization Buffer and used immediately or stored at 4 ºC. The amplification of DNA was performed by PCR. The amplicons were resolved in 1.5% agarose gel by Northern blot. The reagents used for the reaction are listed in Table 21. The amplification protocol used for the PCR reaction is listed in Table 26. The primers used are listed in Table 27.

Table 26 – Protocol used for the PCR reaction: Gt(ROSA)26Sor$^{tm4(ACTB-tdTomato,-EGFP)Luo}$ mice

Reaction	Temperature		Time
Denaturation 1	95 ºC		3 min
Denaturation	36×	95 ºC	30 s
Annealing		62 ºC	60 s

Table 26 - continued

Extension		72 ºC	50 sc
Dissociation	72 ºC		5 s
Storage	4 ºC		Long term

Table 27 – Primers used for the PCR reaction: Gt(ROSA)26Sor$^{tm4(ACTB-tdTomato,-EGFP)Luo}$ mice

Name	Sequence (5'- 3')
Wild type forward	GGAGCGGAAATGGATATG
Common reverse	AAAGTCGCTCTGAHTTGTTAT
Mutant forward	AAGACCGCGAAGAGTTTGTC

4.2.25 Bulk RNA-seq

After fluorescent activated cell sorting (FACS) of 1×10^5 endothelial cells, total RNA was isolated using the RNeasy Plus micro kit (Qiagen, USA, #74034). To avoid genomic DNA contamination, the samples were digested with DNase using the DNase-FreeDNase Set (DNase-FreeDNase Set, Qiagen, USA, #79254). The integrity of RNA and library preparation was verified with LabChip Gx Touch 24 (Perkin Elmer, USA, # CLS138162), using 300 pg of total RNA as input for the SMART®-SeqHT kit (Takara Clontech, Japan, # 634455). The sequencing was performed on the NextSeq500 instrument (Illumina, USA, # SP-104-5506), employing the v2 chemistry. resulting in an average of 20 M reads per library with a 1×75 base pair single-end setup. The quality control for the raw ends was assessed by the FastQC tool (). Only reads between 30 and 150 nucleotides were included in the analysis. The reads were aligned versus the Ensembl mouse genome version mm10 (GRCm38) using the method STAR 2.6.1d with the parameter "outFilterMismatchNoverLmax 0.1" to have a maximum ratio of mismatches to mapped length to 10% (). The number of reads aligning to genes was assessed using the featureCounts 1.6.3 tool from the Subread package. Only reads mapping at least partially inside exons were considered per

gene. Reads overlapping multiple genes or aligning to multiple regions were excluded. Only genes with a minimum fold change of ± 1.5(log2FC ± 0.585) and a maximum Benjamini–Hochberg corrected P value of 0.05 were considered to be differentially expressed. The Ensemble annotation was enriched using the UniProt database (release 06.06.2014), based on the Ensembl gene identifiers database.

4.2.26 Statistical analysis

Statistics and graphs were performed using GraphPad Prism software. Differences between groups were estimated by one-way ANOVA with Tukey's *post hoc* test, or by two-way ANOVA with Bonferroni's multiple comparisons test. Differences between the two groups were assessed with an unpaired Student's t-test. Values are presented as mean ± SD. Outliers were identified by Grubbs' test. *P* values below 0.05 were considered significant.

5 Results

5.1 The Foxo transcription factors gene expression in the lung of newborn mice

Although the Foxo transcription factors are accreditated with a pivotal role in mouse development (32), and the regulation of apoptosis in the pathogenesis of a broad range of diseases (43, 61, 80), to date there is no information on Foxo1, Foxo3, Foxo4 and Foxo6 mRNA expression levels and protein regulation in late lung development. To assess whether hyperoxia could affect gene expression of the Foxo transcription factors in mouse developing lung, wild-type C57BL/6J mice were exposed to either 85% or 21% O_2 from P1 to P14. The lungs were harvested at P14 and total RNA was purified from the lung homogenate. The quantification of the steady-state levels of the Foxo transcription factors mRNA expression was performed by real-time PCR. In mouse lungs subjected to 85% O_2, Foxo1 mRNA levels were significantly downregulated compared to the age-matched controls. Conversely, Foxo3 and Foxo6 mRNA expression resulted significantly upregulated in mice exposed to 85% O_2 at P14. The gene expression of Foxo4 resulted not significantly reduced in hyperoxia if compared with the age-matched controls (Figure 2). Given the essential role of the Foxo transcription factors in normal mouse development, the modulation of the expression of the Foxo transcription factors induced by hyperoxia suggests a role of the Foxo genes in hyperoxia-induced lung injury.

5.2 Variation of the protein abundance and gene expression of Foxo1 during the mouse postnatal lung development

The lungs of postnatal mice exposed to 85% or 21% O_2 were harvested on P5, postnatal day 7 (P7) and P14 to chart the effect of hyperoxia on gene expression and protein abundance of Foxo1 during postnatal lung development. Hyperoxia did not induce any significant reduction in the steady-state mRNA levels of Foxo1 at P5 and P7. Conversely, the mRNA levels of Foxo1 were significantly downregulated only in mice exposed to hyperoxia at P14. The assessment of the protein abundance performed by western blot revealed no significant variation in the total levels of Foxo1 protein in mice exposed to hyperoxia at P5, P7 and P14. The phosphorylation of Foxo1 on S256 resulted significantly decreased only in mice exposed to hyperoxia at P14 compared with the normoxia controls (Figure 3). These data indicate that hyperoxia affects the downregulation of Foxo1 during the alveolar stage of lung development.

5.3 Foxo4 protein expression in an experimental model of BPD

To investigate whether the protein abundancy of Foxo4 in P14 mice exposed to hyperoxia could reflect the mild reduction observed in the gene expression of Foxo4, the protein amount of Foxo4 was assessed by western blot. The analysis of Foxo4 protein levels from the lung of P14 mice exposed to either 85% O_2 or 21% O_2 revealed that hyperoxia induced a statistically significant downregulation of the protein expression of Foxo4 when six replicates per group were considered. Despite the reduction of Foxo4 protein levels in hyperoxia was statistically significant, the average of the values calculated by densitometry account for a difference of 0.3 units. These data suggest that hyperoxia was able to induce only a mild reduction in the protein levels of Foxo4 consistently with the previously observed reduction of Foxo4 mRNA levels (Figure 4).

5.4 Assessment of the expression of genes regulated by Foxo1 according to the literature in mouse lungs exposed to hyperoxia

To study the downstream effect of the downregulation of Foxo1induced by hyperoxia, newborn mice were exposed to either 85% O_2 or 21% O_2, the lungs were harvested on P14 and homogenized to extract total RNA. The gene expression of three genes which are proven by the literature to be regulated by the Foxo1 pathway was analyzed by real-time PCR. The gene expression of cyclin dependent kinase inhibitor 1a (Cdkn1a) and E2f transcription factor 1 (E2f1) were significantly upregulated in P14 mice exposed to hyperoxia compared with the age-matched controls. Conversely, hyperoxia induced a significant downregulation of the steady-state mRNA levels of Cyclin e 1 (Ccne1) in P14 lungs compared to normoxia controls (Figure 5).

5.5 Analysis of the gene expression of the Foxo transcription factors in different cultured mouse pulmonary cells

In order to evaluate whether the steady-state mRNA expression of the Foxo transcription factors could be different comparing different cell types in a cell-culture-based experiment, AT2 cells, PASMCs, and PFBs were isolated from the lung of 9-11 weeks mice. LMECs were purchased from Creative Bioarray (LMECs, Creative Bioarray, USA, # CSC-C1746). PASMCs, LMECs and PFBs were plated at a concentration of 2×10^5 cells/well in a six-well plate, AT2 cells were plated on a permeable insert with a concentration of 2×10^4. After 24 h the cells were harvested and the total RNA extracted. The cDNA was produced to perform real-time PCR analysis. The

gene expression of Foxo1 was significantly higher in LMECs compared to all the other cell types considered. Foxo3 expression was the lowest in LMECs compared with the other cell types. No significant variations in the mRNA levels of Foxo4 were found among the four cell types analyzed. The gene expression of Foxo6 was significantly higher in PASMCs and LMECs compared to the other two cell types analyzed (Figure 6). Despite the limitations of a cell-culture-based experiments, these data suggest that, compared with the other cell types considered, a higher gene expression of Foxo1 is an hallmark of LMECs genetic profile.

5.6 Assessment of the gene expression of the Foxo transcription factors in FACS-sorted cells in a mouse model of BPD

To further identify in which cell types of the lung the gene expression of the Foxo transcription factors was influenced by hyperoxia, newborn mice were exposed to 85% or 21% O_2 and their lungs were harvested at P14 and digested to obtain a single-cell suspension suitable for FACS analysis. Lung endothelial cells were identified using the cluster of differentiation 31 (CD31) as a positive marker the cluster of differentiation 45 (CD45) was used to exclude the immune cells which were double-positive for CD31. Epithelial cells were detected by the epithelial cell adhesion molecule (EpCAM). To include the other cell types which were not detected by any surface marker, a "rest" channel was employed. Therefore, live cells negative for CD31, EpCAM and CD45, were sorted together as part of the rest channel. The mRNA levels Foxo1 were downregulated only in lung microvascular endothelial cells FACS-sorted from P14 lungs exposed to hyperoxia compared with the age-matched controls. The steady-state mRNA expression of Foxo1 in normoxia was higher in the endothelial cells compared with the other cell types considered. No significant changes in the gene expression of Foxo1 were found in epithelial, immune cells or the rest fraction. Hyperoxia did not induce any significant change in the mRNA expression of Foxo3, Foxo4 and Foxo6 in any of the cell types considered (Figure 7). These data indicate that the high expression of Foxo1 is part of the genetic signature of normoxic endothelial cells in the P14 lung consistently with the line of evidence previously found comparing different cell types cultivated in cell culture. Furthermore, hyperoxia affected the gene expression of Foxo1 only in endothelial cells in a mouse model of BPD, suggesting that among the four Foxo transcription factors, hyperoxia was able to affect only on the expression of the Foxo1 gene in the postnatal lung.

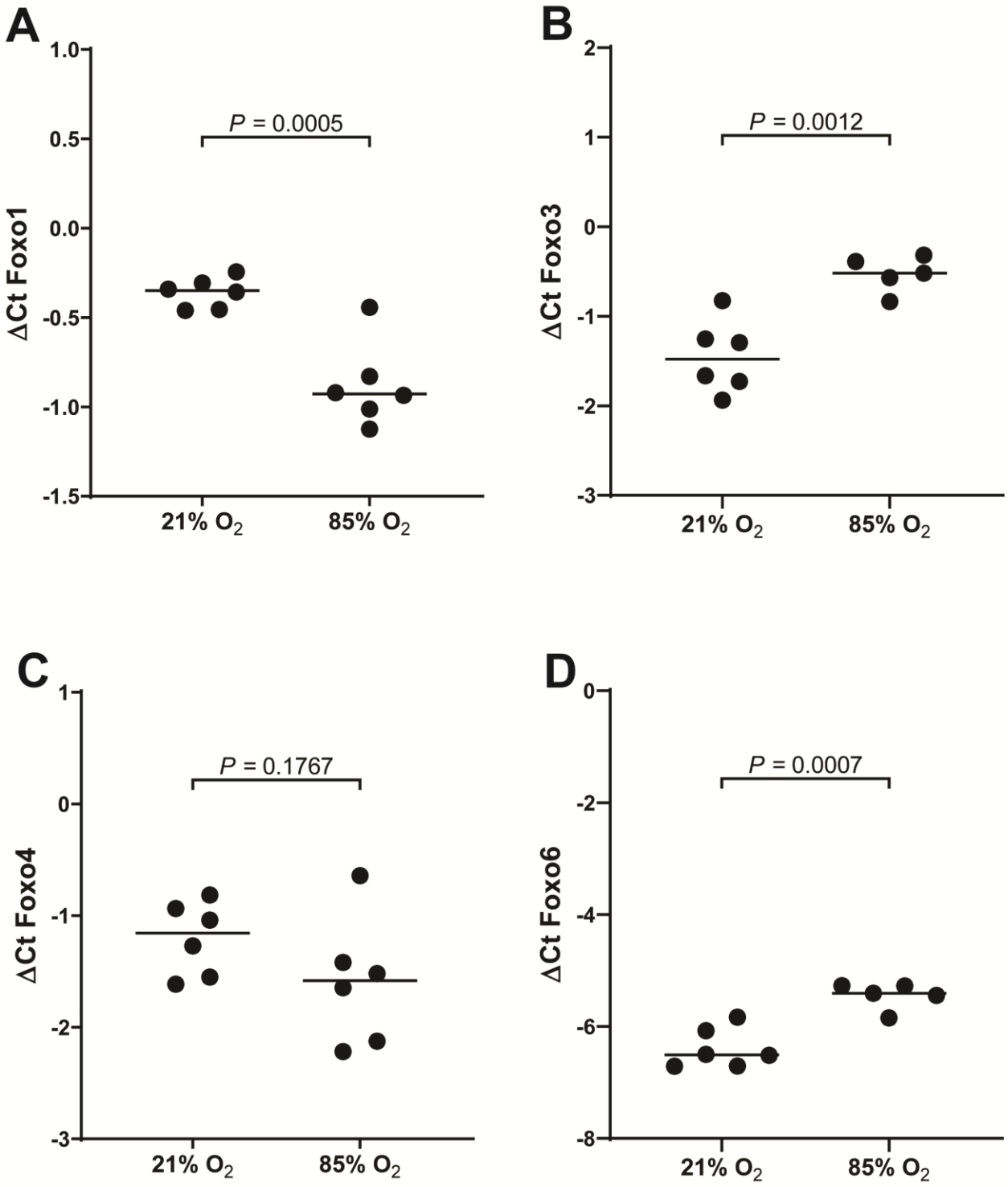

Figure 2 - The Foxo transcription factors gene expression in the lung of newborn mice. The gene expression of Foxo1 (A), Foxo3 (B), Foxo4 (D) and Foxo6 (E) were evaluated by real-time PCR in lungs from P14 mice exposed to 21% or 85% O_2. The RNA polymerase gene was used as a reference. Data represent the mean of ΔCt ± SD. The *P* values were calculated by unpaired Student's *t*-test.

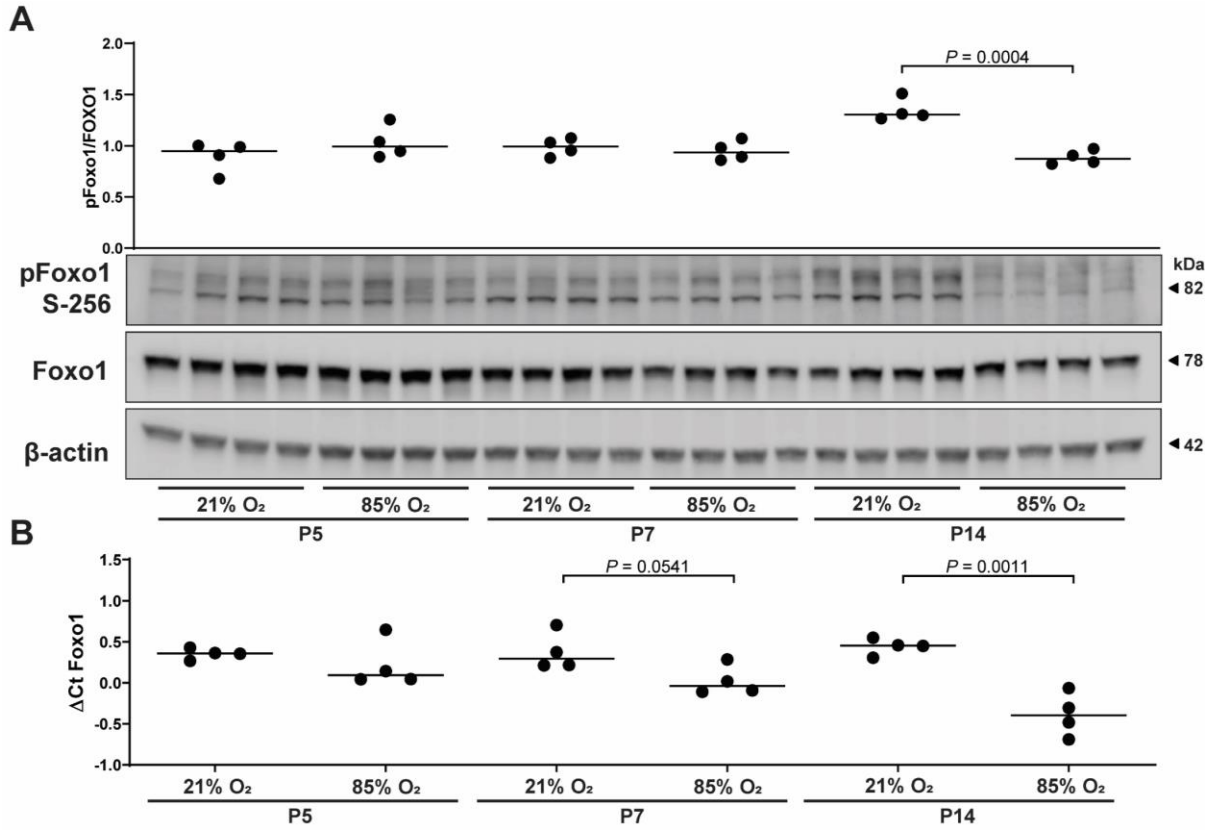

Figure 3 - Variation of the protein abundance and gene expression of Foxo1 during the mouse postnatal lung development. Representative immunoblot of Foxo1 and pFoxo1 over the postnatal late lung development (A). The β-actin was used as a loading control. Gene expression of Foxo1 over the late lung development (B). The RNA polymerase gene was used as a reference. Lungs of newborn mice exposed to 21% or 85% O_2 were harvested at P5, P7 and P14. The data of the gene expression quantification represent the mean of ΔCt ± SD. The *P* values were calculated by unpaired Student's *t*-test.

5.7 The number of lung endothelial cells is significantly reduced in a mouse model of BPD

The lungs of P14 mice exposed to 85% O_2 or 21% O_2 were harvested and digested to produce a single-cell suspension to assess the effect of hyperoxia on the proportion of endothelial cells in the lung of P14 mice. Endothelial cells were detected with CD31, CD45 was used as exclusion marker of the immune cells positive for CD31. The discrimination between live and dead cells was performed with DAPI. The relative number of $CD31^{+}/CD45^{-}/DAPI^{-}$ cells was quantified by flow cytometry. Hyperoxia induced a significant reduction in the percentage of endothelial cells in the lung of P14 mice comparing with the age-matched controls. These findings outline that hyperoxia affects significantly the percentage of endothelial cells in the lung of P14 mice in the context of a mouse model of BPD (Figure 7).

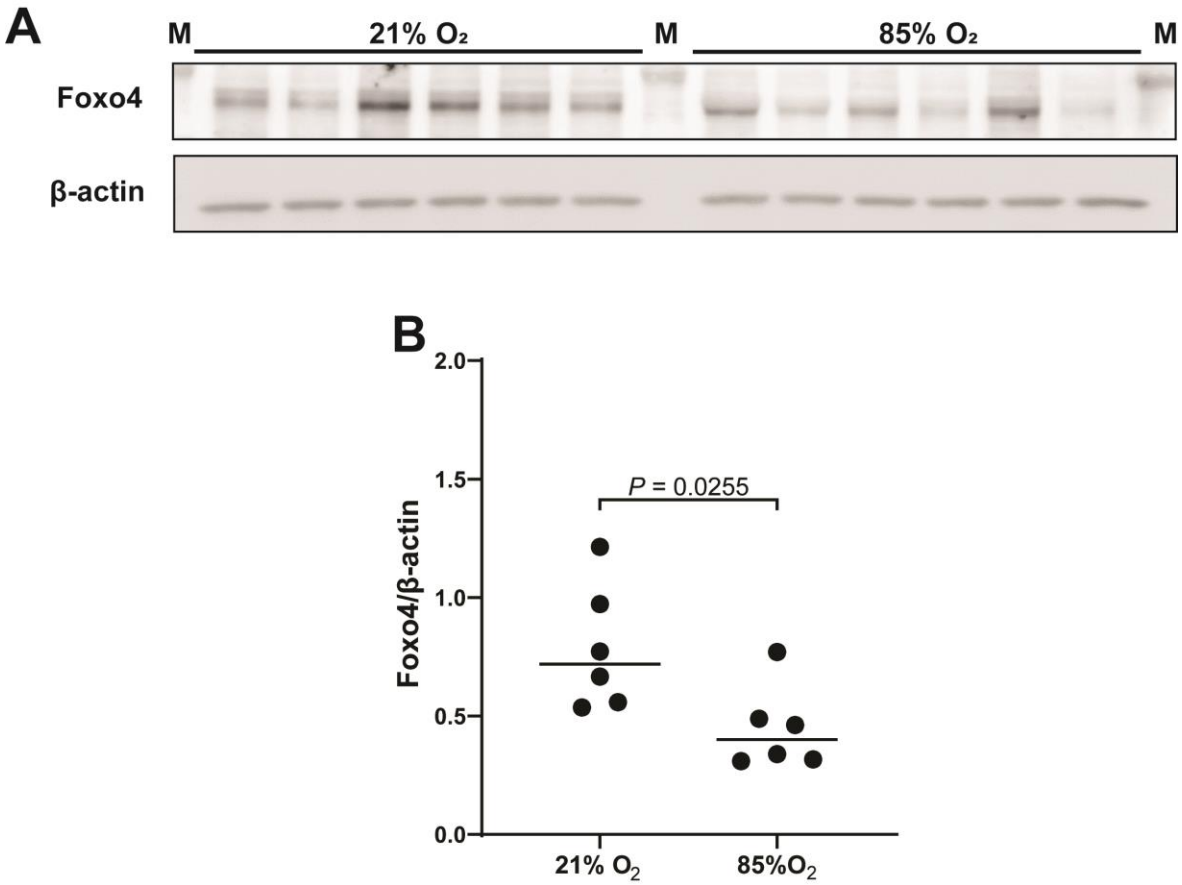

Figure 4 - Foxo4 protein expression in an experimental model of BPD. Representative immunoblot of Foxo4 protein expression in P14 lungs from mice exposed to 21% or 85% O_2 (A and B). The β-actin was used as loading control. The data represent the mean of ΔCt ± SD. The *P* values were calculated by unpaired Student's *t*-test. M, marker.

5.8 Analysis of the transcriptome of FACS-sorted lung endothelial cells in a mouse model of BPD

To investigate the effect of hyperoxia on the gene expression in lung endothelial cells of P14 mice, endothelial cells were FACS-sorted from the lung of newborn mice exposed to 85% or 21% O_2. For each condition, $1x10^5$ cells were collected from three independent mice per group and the total RNA was purified from each sample. Transcriptomic analysis revealed a consistent impact of hyperoxia in the regulation of the apoptosis pathways in lung endothelial cells *in vivo*. Endothelial cells sorted from newborn mice exposed to hyperoxia were characterized by the upregulation of some important genes belonging to the intrinsic pathway of apoptosis such as Bcl2 associated x regulator 1 (Bax1) and Bcl2 antagonist killer 1 (Bak1). Conversely, the gene expression of the extrinsic effectors of apoptosis Caspase 2, 6, 7, 8 and 9 was downregulated as well as the downstream apoptosis mediator Poly (ADP-Ribose) polymerase 1 (Parp1) (Figure 9).

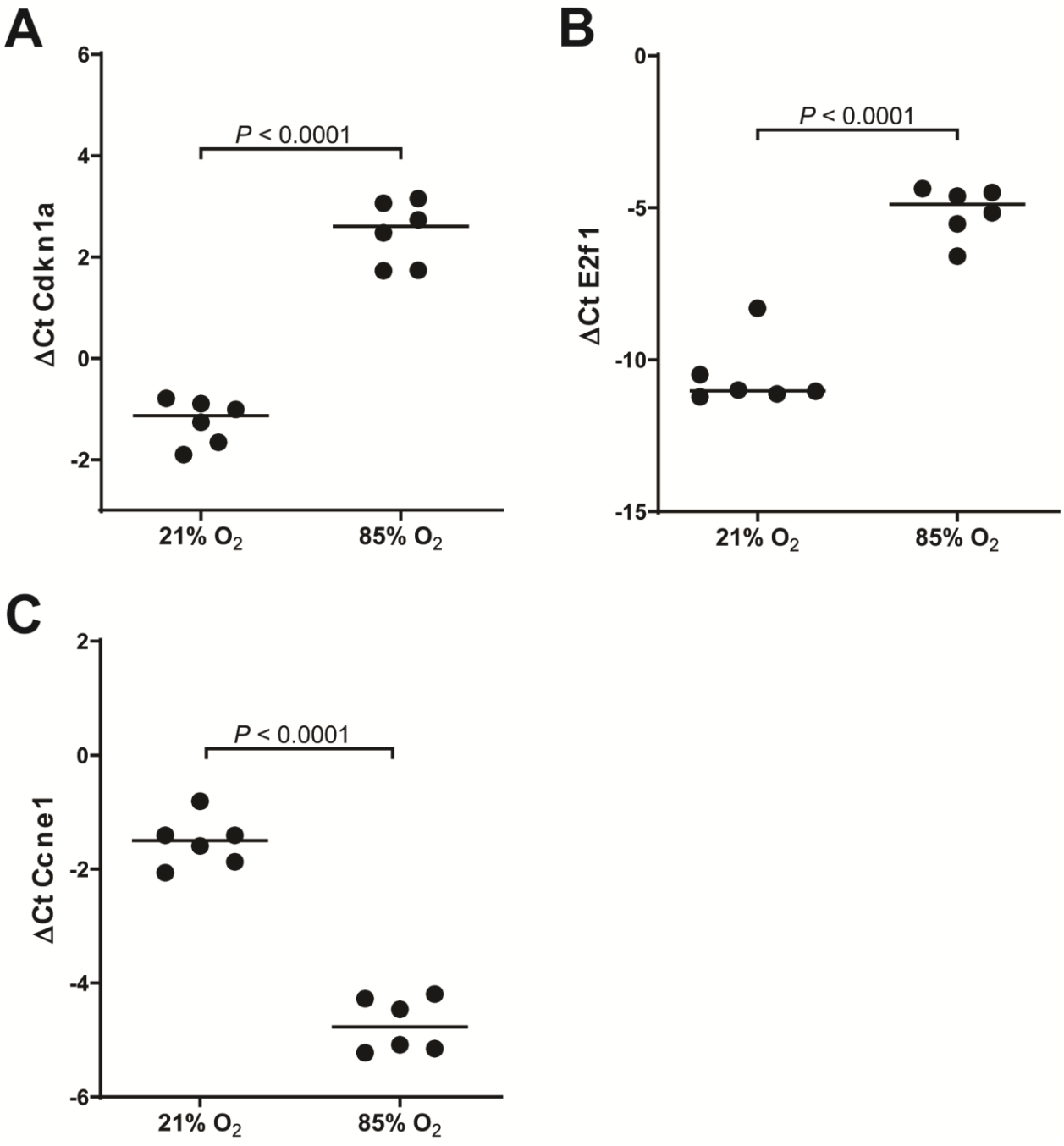

Figure 5 - Assessment of the expression of genes regulated by Foxo1 according to the literature in mouse lungs exposed to hyperoxia. The gene expression of Cdk1a (A), E2f1 (B) and Ccne1 (D) were assessed by real-time PCR in lungs from P14 mice exposed to 21% or 85% O_2. The RNA polymerase gene was used as a reference. The data represent the mean of ΔCt ± SD. The *P* values were calculated by unpaired Student's *t*-test.

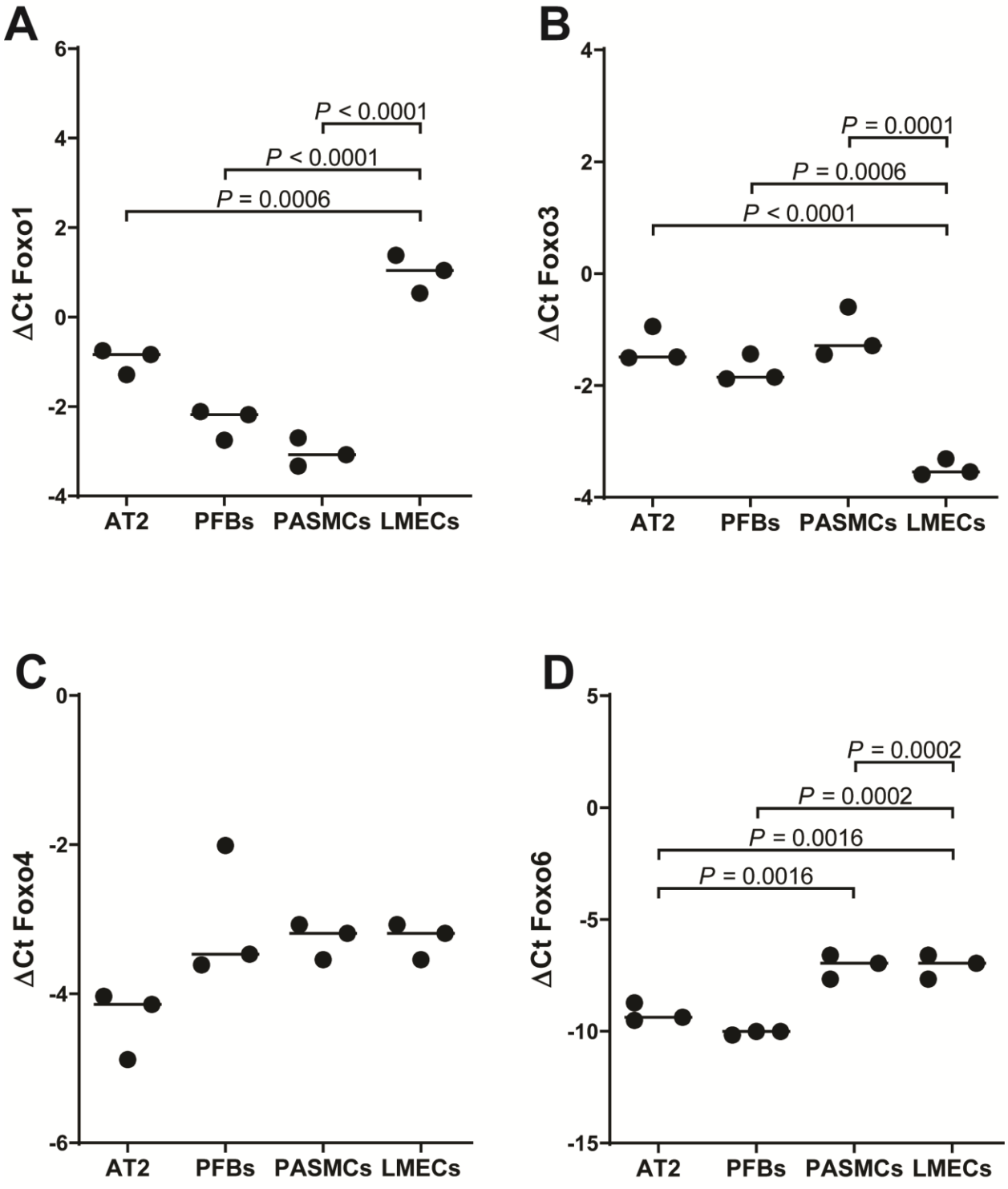

Figure 6 - Analysis of the gene expression of the Foxo transcription factors in different cultured mouse pulmonary cells. The mRNA expression of Foxo1 (A), Foxo3 (B), Foxo4 (C), and Foxo6 (D) was assessed by real-time PCR from epithelial cells (AT2), pulmonary fibroblasts (PFBs), pulmonary arthery smooth muscle cells (PASMCs) and lung microvascular endothelial cells (LMECs). The cells were cultured for 24 h after isolation. The data represent the mean of ΔCt ± SD. The *P* values were calculated by one-way ANOVA with Tukey's *post hoc* test.

5.9 Employment of the Tie2-Cre endothelial-specific driver to assess the role of Foxo1 perturbations in lung endothelial cells in normal and aberrant late lung development

The Tie2-Cre lung endothelial-specific driver was crossed with the mTmG reporter line to assess the yield of activation in Tie2 expressing cells in the postnatal lung. Newborn mice were injected with tamoxifen 0.1 µg per mouse on P3 and P4 and the lungs were harvested on P14. From the P14 lungs, was produced a single-cell suspension which was analyzed by flow cytometry. Quantification by flow cytometry revealed that tamoxifen activated efficiently the expression of GFP in P14 lungs. The percentage of GFP^+ cells in the lung of tamoxifen-treated P14 mice was twenty times higher compared to the age-matched controls. (Figure 10). These data demonstrate the effectiveness of the tamoxifen administration chosen to activate the Tie2-Cre endothelial-specific driver in P14 mice. These studies were not repeated under hyperoxia.

5.10 Impact of early apoptosis in lung microvascular endothelial cells exposed to hyperoxia *in vivo*

The bulk RNA-seq analysis previously described (Figure 9), showed that hyperoxia induced not only the upregulation of genes such as Bax1, Bak1 and B-cell lymphoma 2l1 (Bcl2l1) involved in the activation of the intrinsic pathway of apoptosis, but also a significant reduction in genes belonging to the extrinsic pathway such as Caspase 2, 6, 7, 8 and 9. To identify the pathway ruling the effect of hyperoxia in modulating apoptosis in lung endothelial cells from newborn mice, the lungs of P14 mice exposed to either 85% O_2 or 21% O_2 were used to produce a single cell suspension. Endothelial cells were identified using CD31 as a pan-endothelial marker. The immune marker CD45 was employed to exclude immune cells positive for CD31. The detection of early apoptosis cells was performed with AnnexinV. The discrimination between live and dead cells was performed using DAPI. After the staining, the cells were analyzed by flow cytometry. In the lung of P14 mice exposed to hyperoxia, a significant reduction in the percentage of endothelial cells which were positive to AnnexinV was observed compared with the normoxia control. These findings, taken together, suggest that hyperoxia downregulated early apoptosis signalling in lung endothelial cells from P14 mice. The downregulation of key genes involved in the extrinsic apoptosis cascade resulted in the main genetical perturbation involved in the hyperoxia-mediated downregulation of the apoptotic signalling in lung endothelial cells from P14 mice (Figure 11).

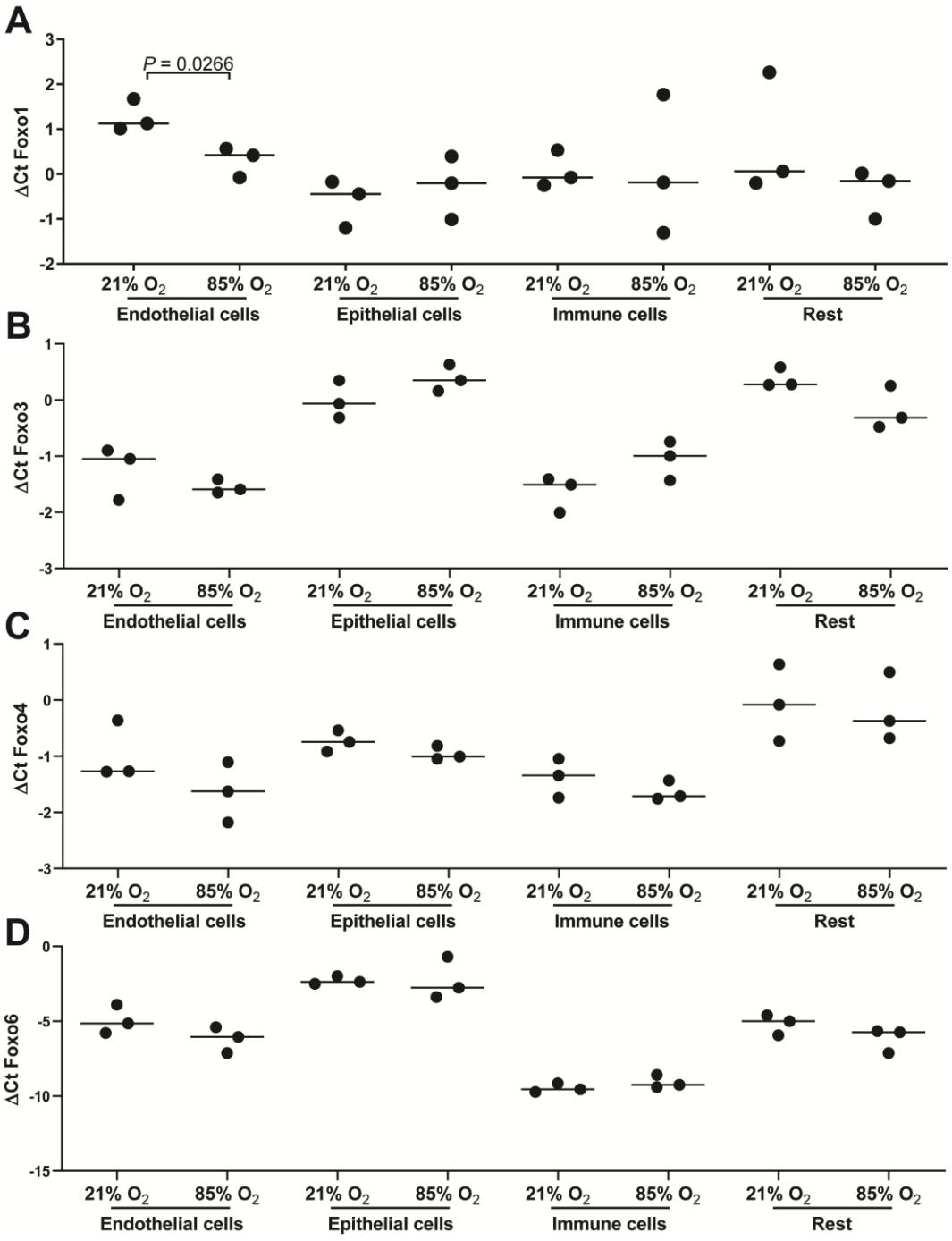

Figure 7 - Assessment of the gene expression of the Foxo transcription factors in FACS-sorted cells in a mouse model of BPD. The mRNA expression of Foxo1 (A), Foxo3 (B), Foxo4 (C), and Foxo6 (D) were assessed by real-time PCR from FACS-sorted cells isolated from P14 lungs exposed to 21% or 85%O_2. CD31 (cluster of differentiation 31) was used to select the endothelial cells using CD45 (cluster of differentiation 45) as exclusion marker of the $CD31^+$ immune fraction. EpCam (epithelial cell adhesion molecule) was used to sort the epithelial cells. CD45 was used as pan-immune marker for the immune cells. The populations not labelled with specific markers were sorted as a Rest. The data represent the mean of ΔCt ± >SD. The *P* values were calculated by one-way ANOVA with Tukey's *post hoc* test.

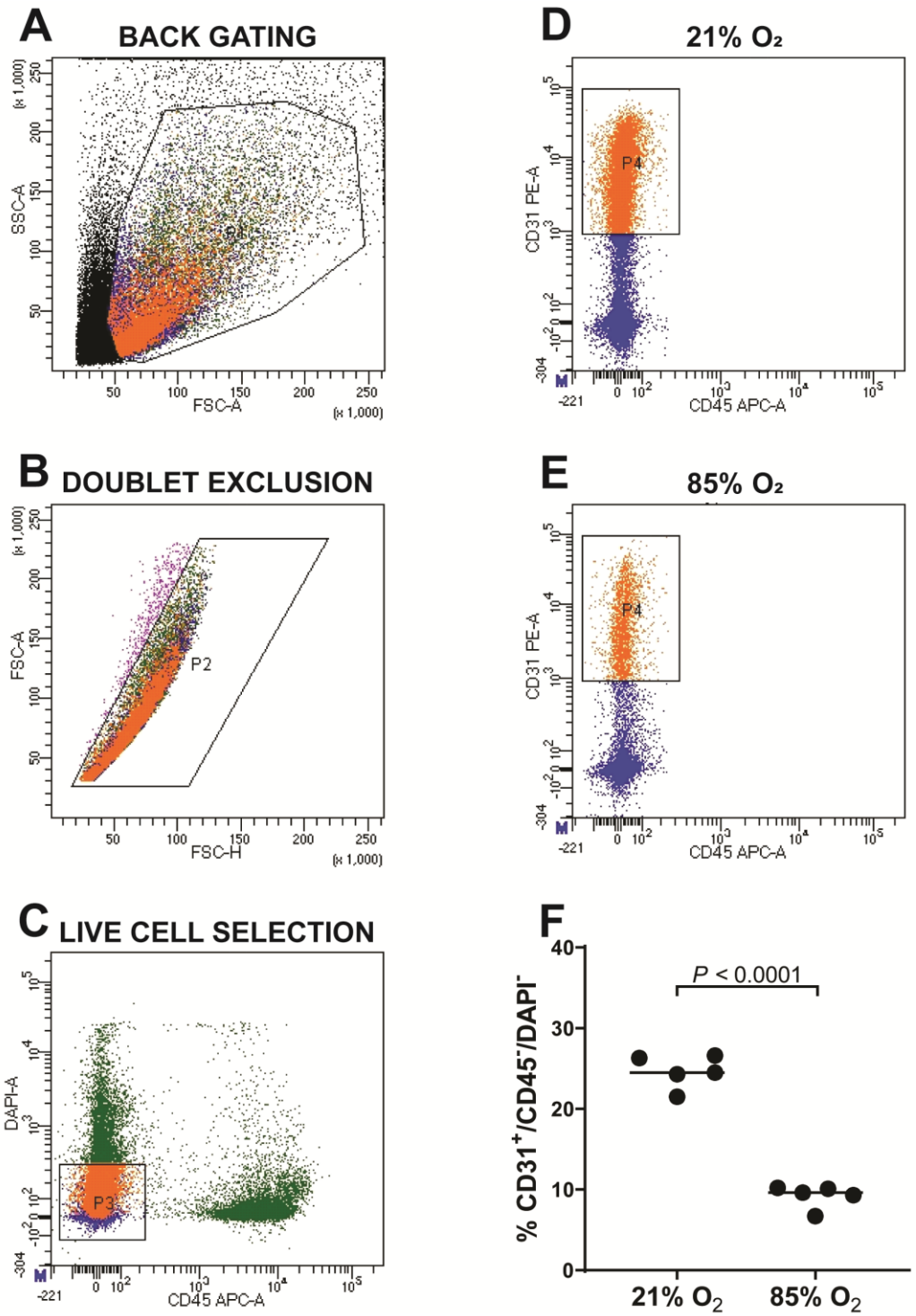

Fgure 8 - The number of lung endothelial cells is significantly reduced in a mouse model of BPD. Endothelial cells were sorted using CD31 (cluster of differentiation 31) as a positive and CD45 (cluster of differentiation 45) as a negative marker. DAPI was used as live/dead discriminator. The quantification of the percentage of endothelial cells was performed by FACSDiva softwere. Data represent the mean of ΔCt ± SD. The *P* value was calculated by unpaired Student's *t*-test. APC, allophycocyanin; PE, phycoerythrin; DAPI, 4′,6-diamidino-2-phenylindole. FSC-A, forward scatter area; FSC-H, forward scatter high; SSC-A; side scatter area.

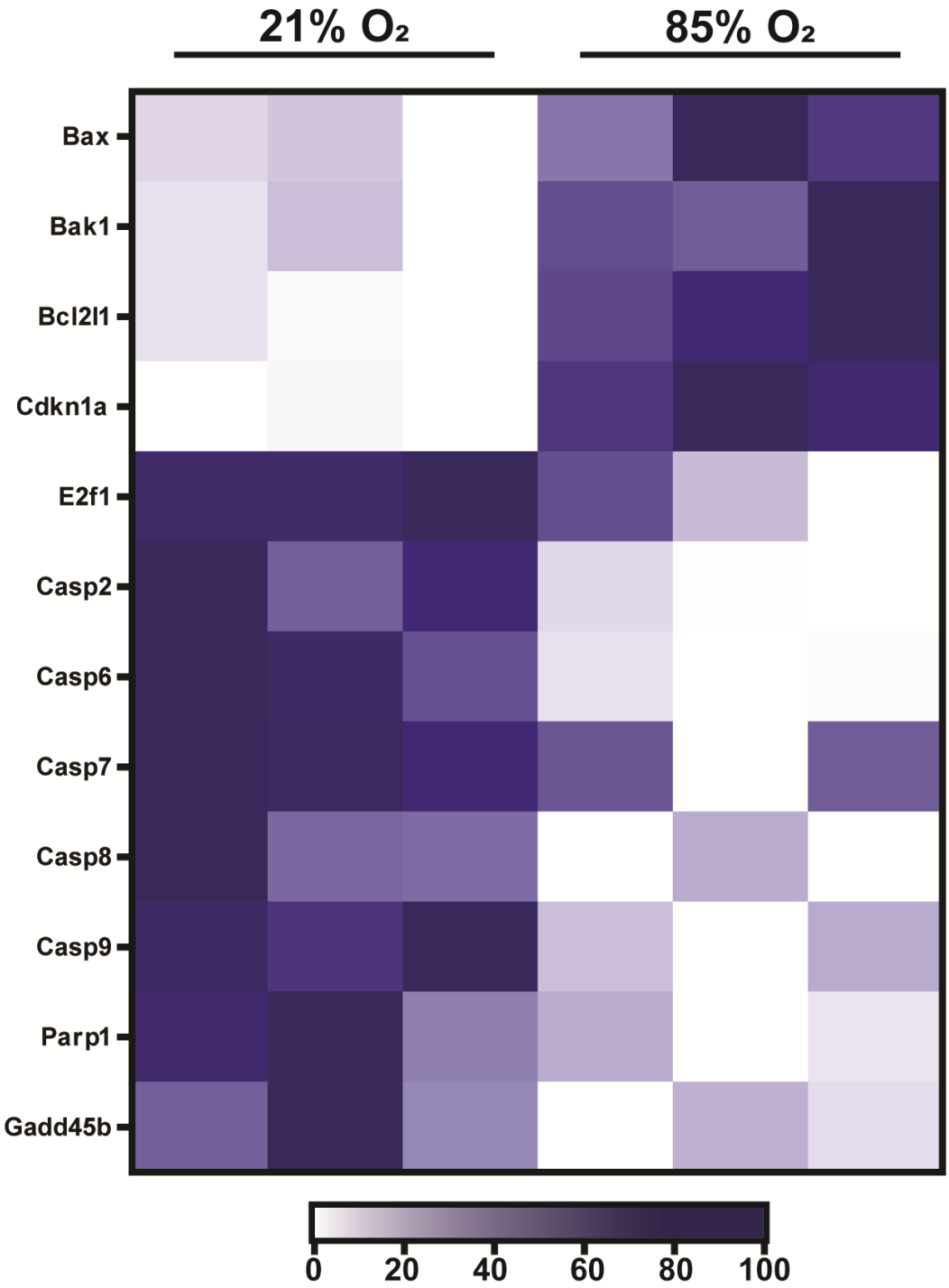

Figure 9 - Analysis of the trascriptome of FACS-sorted lung endothelial cells in a mouse model of BPD. Batch RNA-seq was employed to analyze the impact of hyperoxia on lung endothelial cells FACS-sorted from the lung of P14 mice exposed to 21% or 85% O_2. Bax, Bcl2 associated x regulator 1; Bak1, Bcl2 antagonist killer 1; Bcl2l1, B-cell lymphoma 2l1; Cdkn1a, cyclin dependent kinase inhibitor 1a; E2f1, E2f transcription factor 1; Casp2, Caspase 2; Casp6, Caspase 6; Casp7, Caspase 7; Casp8, Caspase 8; Casp9, Caspase 9; Parp1, Poly (ADP-ribose) polymerase 1; Gadd45b, growth arrest and DNA damage inducible protein 45 b.

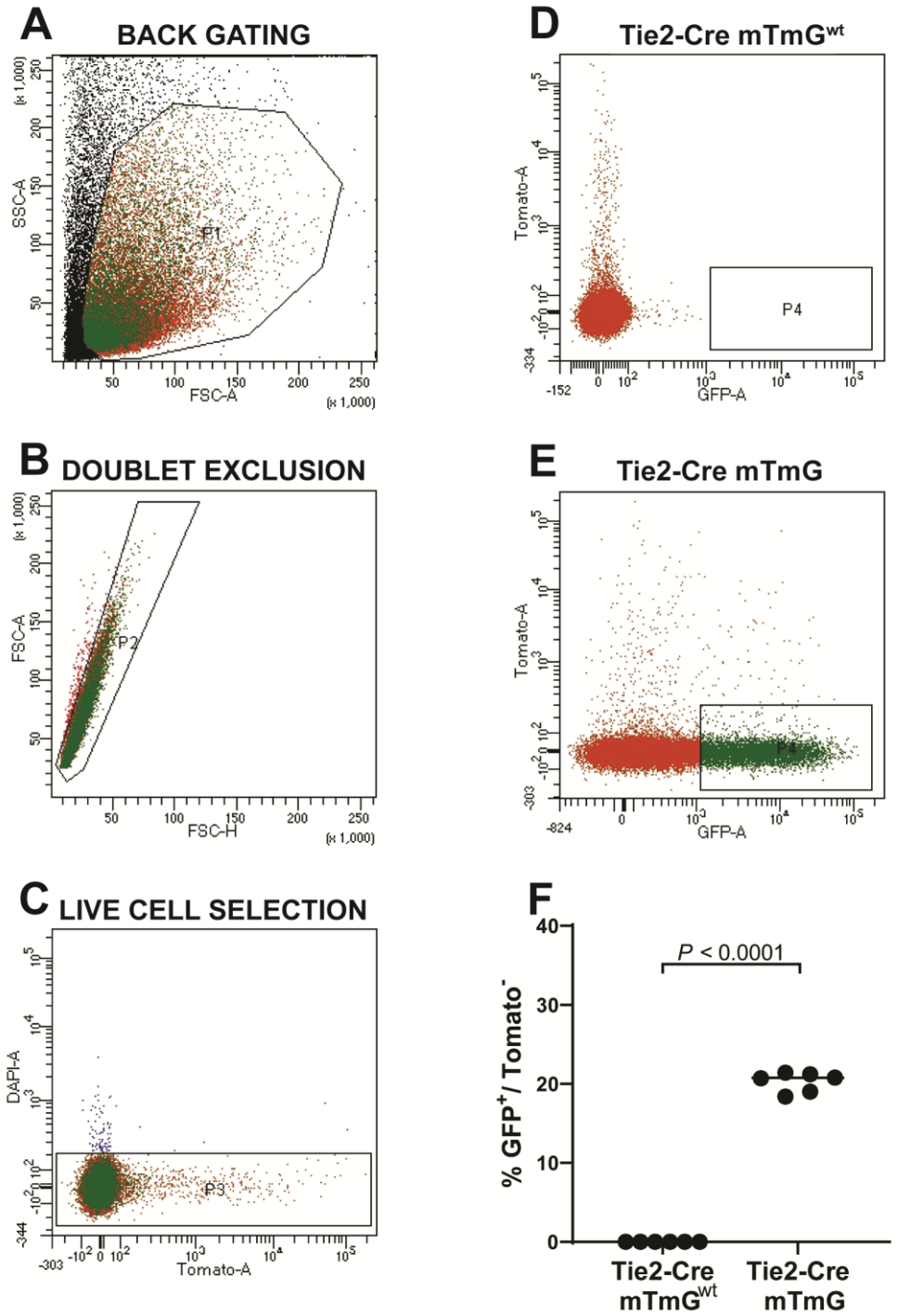

Figure 10 - Employment of the Tie2-Cre endothelial-specific driver to assess the role of Foxo1 perturbations in lung endothelial cells in normal and aberrant late lung development. Gating strategy for the assessment of GFP^+ (green fluorescent protein) cells in P14 Tie2-Cre mTmG mice. The quantification of the percentage of GFP^+ cells was performed by FACSDiva software. Data represent the mean of $\Delta Ct \pm SD$. The *P* value was calculated by unpaired Student's t-test. DAPI, 4′,6-diamidino-2-phenylindole. FSC-A, forward scatter area; FSC-H, forward scatter high; SSC-A; side scatter area; mT, membrane-targeted tandem dimer tomato; mG, membrane-targeted green fluorescent protein.

5.11 Impact of the conditional downregulation of Foxo1 on the body mass of postnatal mice

After generating the Tie2-Cre Foxo1^{ff} line, newborn mice were injected with 0.1 µg tamoxifen per mouse on P3 and P4. To assess the effect of tamoxifen on the gene expression of Foxo1, the lungs of P14 mice were harvested and digested to generate a single cell suspension. The samples were stained with CD45 and EpCAM which were labelled with APC. To enreach in endothelial cells, the immune and epithelial fractions were depleted using magnetic beads conjugated with an anti-APC antibody. The depletion was performed using the AutoMacs magnetic cytometer. The effect of tamoxifen on the steady-state mRNA levels of Foxo1 was analyzed by real-time PCR (Figure 12A). Tamoxifen induced a significant downregulation of the gene expression of Foxo1 in lung specimens enriched in endothelial cells from P14 mice. The conditional downregulation of Foxo1 in Tie2-Cre Foxo1^{ff} mice presented a significant reduction in the body mass of the mice compared with the age-matched controls. In Tie2-Cre Foxo1^{ff} mice injected with 0.1 µg tamoxifen on P3 and P4, the downregulation of Foxo1 induced a significant reduction of the body mass (Figure 12 B). These data suggest that the downregulation of Foxo1, having an impact on regulating the body weight of newborn mouse pups, affects the normal development of the mouse.

5.12 Effect of the conditional downregulation of Foxo1 in lung endothelial cells on the lung structure

To quantify the effect of the conditional abrogation of Foxo1 in lung endothelial cells of P14 mice on the lung structure, Tie2-Cre Foxo1^{ff} and Tie2-Cre Foxo1^{wt} mice were treated with tamoxifen 0.1 µ on P4 and P5. Newborn mice were sacrificed on P14 and the lungs were used for stereological analysis. The conditional downregulation of Foxo1 in lung endothelial cells of P14 mice arrested alveolarization reducing surface area by 40%. Alveolar density and alveoli number were as well reduced by 20%. The mean linear intercept was increased by 20% and septal thickness by 10% in Tie2-Cre Foxo^{ff} mice in comparison with the Tie2-Cre Foxo1^{wt} group (Figures 13 and 14). In the contest of stereological quantification, the hallmarks of the 85 O_2 hyperoxia-based mouse model of BPD are: reduced surface area, alveolar density and alveoli number as well as increased septal thickness and mean linear intercept. Therefore, these findings suggest that the conditional endothelial deletion of Foxo1 in the lung of newborn mice induced an effect of arrested lung development characterized by a simplification in the architecture of the lung which was comparable with the typical phenotype observed in the hyperoxia-based mouse model of BPD.

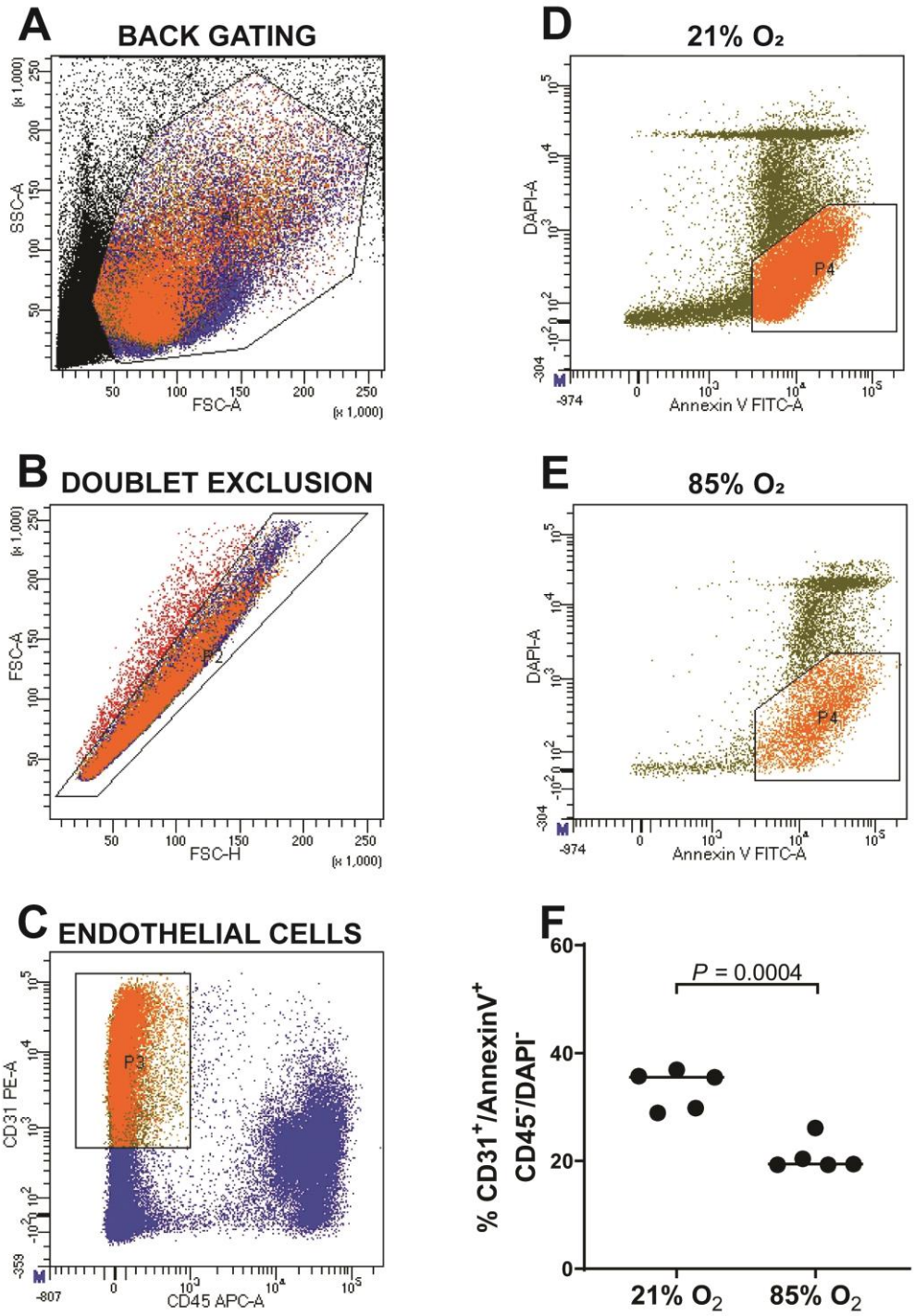

Figure 11 - Impact of early apoptosis in lung microvascular endothelial cells exposed to hyperoxia *in vivo*. Lung endothelial cells from the lung of P14 mice exposed to 21% or 85% O_2 were identified using CD31 (cluster of differentiation 31) as positive and CD45 (cluster of differentiation 45) as as negative marker. Annexin V was used to identify early apoptotic endothelial cells. DAPI was used as live/dead discriminator. The quantification was performed by FACSDiva software. Data represent the mean of ΔCt ± SD. The *P* value was calculated by unpaired Student's *t*-test. APC, allophycocyanin; PE, phycoerythrin; DAPI, 4′,6-diamidino-2-phenylindole. FSC-A, forward scatter area; FSC-H, forward scatter high; SSC-A; side scatter area.

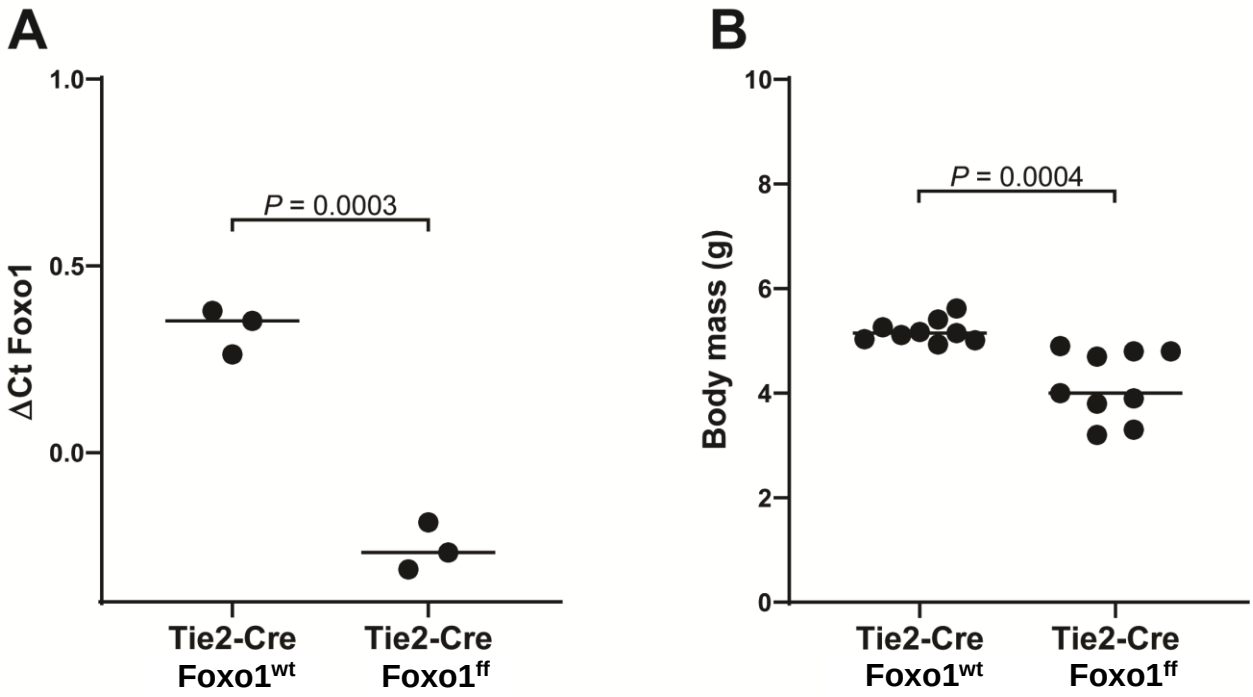

Figure 12 - Impact of the conditional downregulation of Foxo1 on the body mass of postnatal mice. Assessment of the downregulation of Foxo1 in Tie2-Cre Foxo1^{ff} mice (A). Measurement of the body mass in Tie2-Cre Foxo1^{wt} and Tie2-Cre Foxo1^{ff} mice (B). The RNA polymerase gene was used as a reference. The data represent the mean of ΔCt ± SD. The *P* values were calculated by unpaired Student's *t*-test. g, gram.

5.13 Apoptosis response of the downregulation of Foxo1 in lung endothelial cells of newborn mice *in vivo*

To define whether the conditional downregulation of Foxo1 was involved in the modulation of the early apoptosis signalling in lung endothelial cells of newborn mice. Newborn Tie2-Cre Foxo^{ff} mice were treated with 0.1 µg of tamoxifen or vehicle on P4 and P5. On P14 the lungs were harvested and digested to produce a single-cell suspension suitable for flow cytometry analysis. The cells were stained with CD31 to detect the endothelial cells, CD45 to exclude the immune cells expressing also CD31 and Annexin V was used to identify the early apoptotic cells. The live-dead discrimination was performed with DAPI. Flow cytometry quantification showed that the downregulation of Foxo1 in the endothelial cells during the development of the lung induced a significant downregulation of the early apoptotic signalling in comparison with the age-matched controls (Figure 15). These data indicate that the genetic expression of Foxo1 is crucial for the activation of early apoptosis signalling pathways typical of endothelial cells in normal lung development.

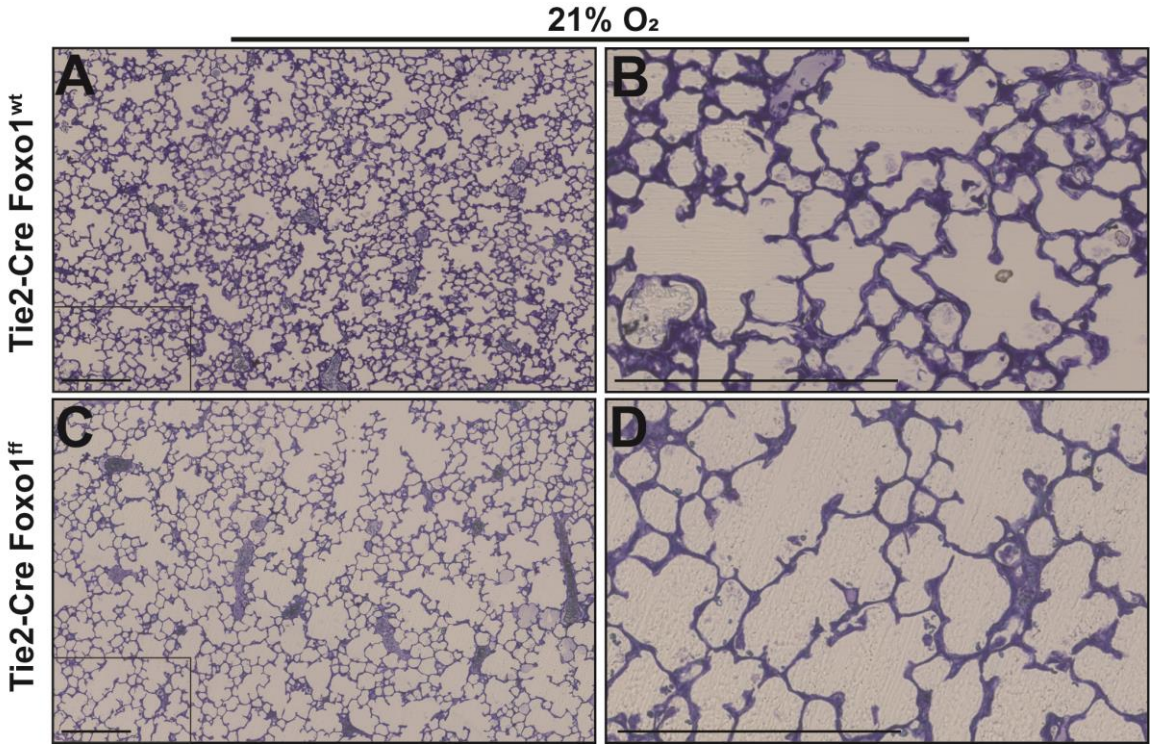

Figure 13 - Effect of the conditional downregulation of Foxo1 in lung endothelial cells on the lung structure. Representative mouse lung tissue sections from P14 Tie2-Cre Foxo1^{wt} (A,B) or Tie2-Cre Foxo1^{ff} (B,C) mice exposed to 21% or 85% O_2.

5.14 Transcriptomic analysis of endothelial cells depleted from the lung of Tie2-Cre Foxo^{ff} mice

Transcriptomic analyses were conducted to define which apoptosis-related genes were modulated by Foxo1 downregulation in endothelial cells. Tie2-Cre Foxo^{ff} mice treated with 0.1 µg tamoxifen or vehicle on P4 and P5 were sacrificed at P14. After digesting the lung to have a single cell suspension, the cells were stained with EpCAM and CD 45 labelled with APC. The epithelial and immune fractions were depleted using a magnetic bead-coupled anti-APC antibody. The depletion, performed with AutoMacs, was used to obtain an enrichment in endothelial cells excluding the main contaminating populations. After the depletion, the cells were centrifuged and the total mRNA extracted. Gene expression analysis performed by bulk RNA-seq highlighted that the downregulation of Foxo1 induced the modulation of genes known to be involved in the apoptotic signallings. The genetic abrogation of Foxo1 in Tie2-Cre Foxo^{ff} mice induced a significant reduction in the gene expression of Parp1, E2f1 and Ccne1 while Cdkn1a and Bcl2l1 were upregulated when compared to the age-matched controls (Figure 16).

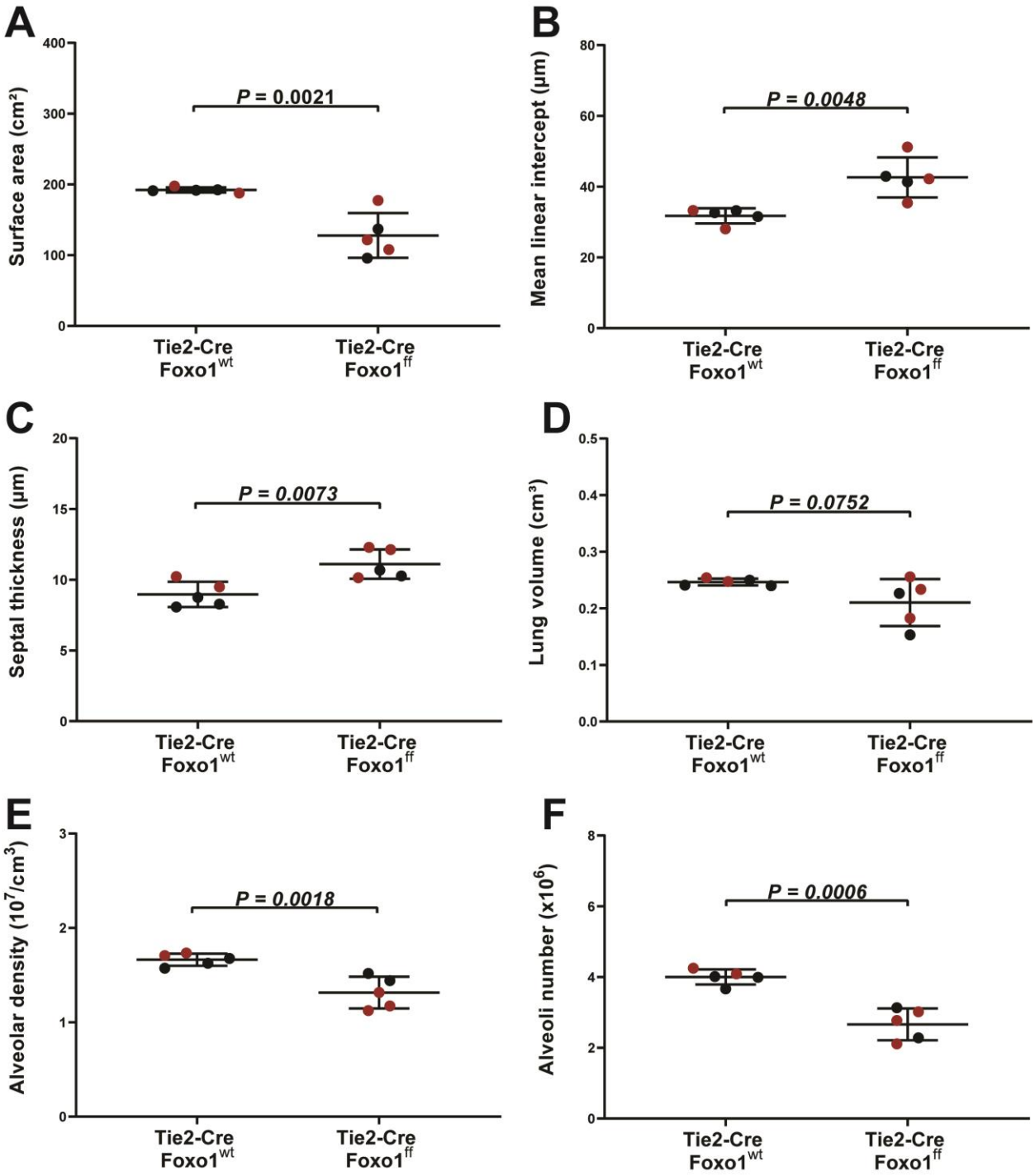

Figure 14 - Impact of the conditional downregulation of Foxo1 in lung endothelial cells on the lung structure. Design-based Stereology was employed to assess surface area (A), mean linear intercept (B), septal thickness (C), alveolar density (E), alveoli number (F). The lung volume (D) was measured using Cavalieri method. The data represent the mean of ΔCt ± >SD. The data represent the mean of ΔCt ± >SD. The *P* values were calculated by unpaired Student's *t*-test. red dot, female; black dot, male; wt, wildtype; ff, floxed.

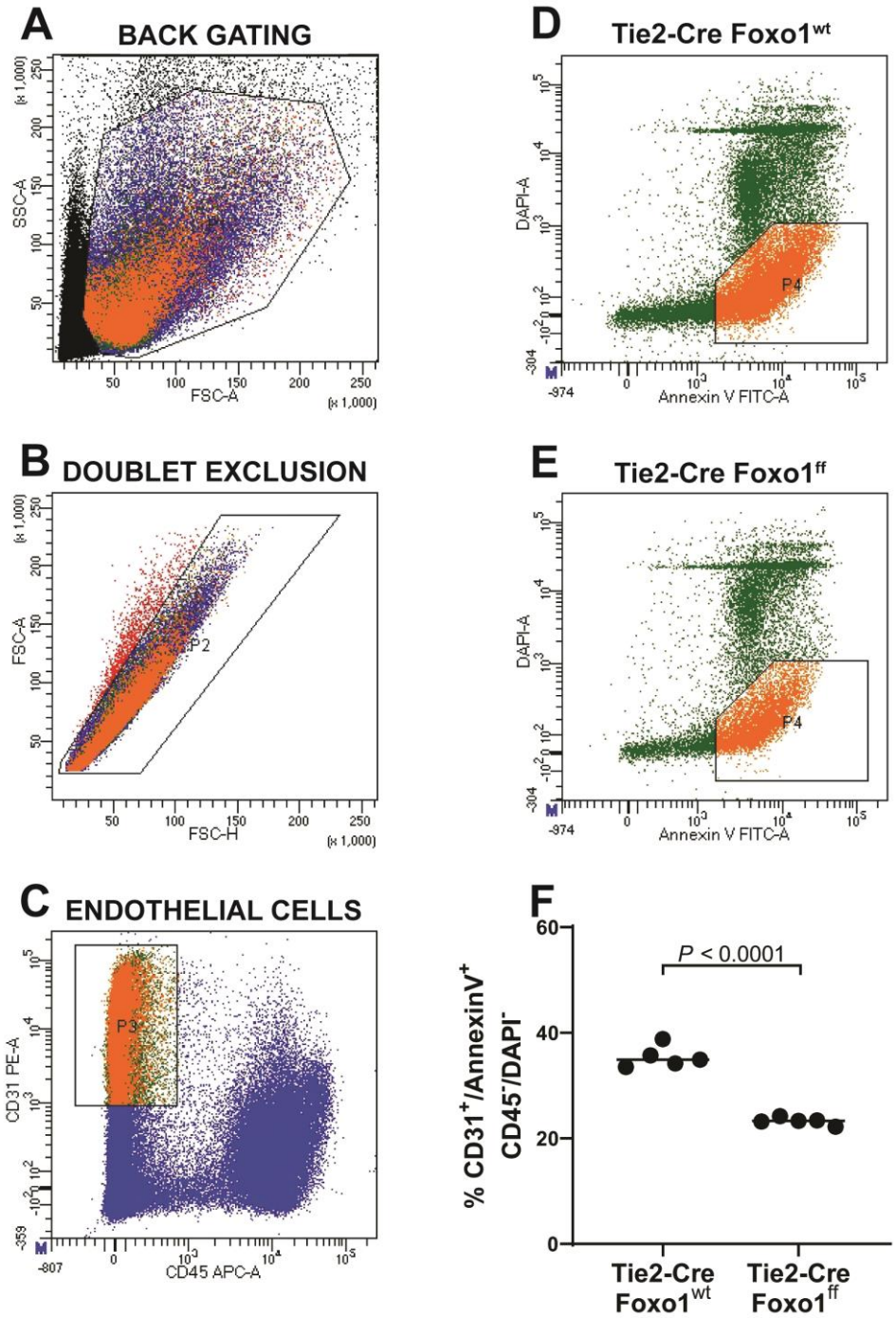

Figure 15 - Impact of the downregulation of Foxo1 on apoptosis in lung endothelial cells of newborn mice *in vivo*. Lung endothelial cells from the lung of P14 Tie2-Cre Foxo1^{wt} or Tie2-Cre Foxo1^{ff} mice exposed to 21% or 85% O_2 were identified using CD31 (cluster of differentiation 31) as positive and CD45 (cluster of differentiation 45) as negative marker. Annexin V was used to identify early apoptotic endothelial cells. DAPI was used as live/dead discriminator. The quantification was performed by FACSDiva softweae. Data represent the mean of ΔCt ± SD. The *P* value was calculated by unpaired Student's *t*-test. APC, allophycocyanin; PE, phycoerythrin; DAPI, 4′,6-diamidino-2-phenylindole. FSC-A, forward scatter area; FSC-H, forward scatter high; SSC-A; side scatter area.

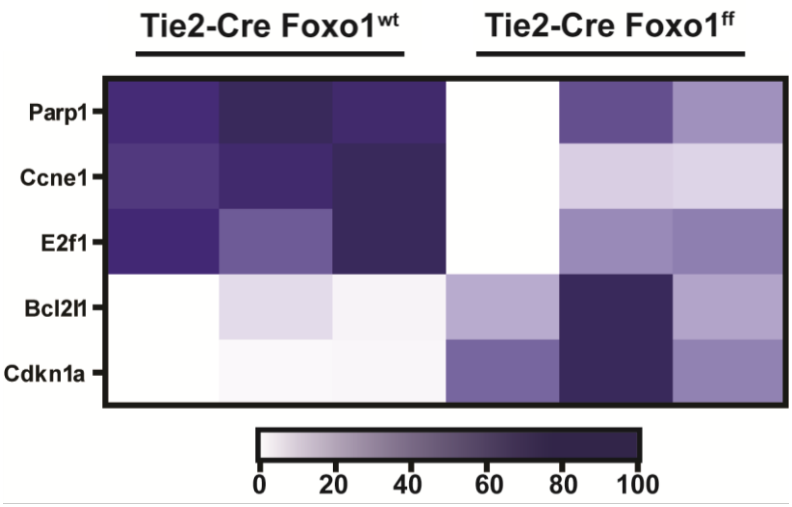

Figure 16 - Transcriptomic analysis of endothelial cells depleted from the lung of Tie2-Cre Foxo^{ff} mice. Batch RNA-seq was employed to analyze the impact of hyperoxia on lung endothelial cells FACS-sorted from the lung of P14 mice exposed to 21% or 85% O_2. Bcl2l1, B-cell lymphoma 2l1; Cdkn1a, cyclin dependent kinase inhibitor 1a; E2f1, E2f transcription factor 1; Parp1, Poly (ADP-ribose) polymerase 1; Cdkn1a, cyclin dependent kinase inhibitor 1a

5.15 Impact of the conditional upregulation of Foxo1 in lung endothelial cells on the lung structure in a mouse model of BPD

To further evaluate the effect of the gene expression of Foxo1 in endothelial cells during postnatal lung development and in a mouse model of BPD, newborn Tie2-Cre Foxo1^{oe} and Tie2-Cre Foxo1^{wt} mice were injected with 0.1 µg tamoxifen per mouse or the same volume of NaCl on P1 and P2 and exposed to 85% O_2 or 21% O_2. The conditional upregulation of Foxo1 in lung endothelial cells protected alveolarization from hyperoxia, increasing surface area by 20%, reducing mean linear intercept by 30%, alveolar density by 20% and alveoli number by 30% (Figures 17 and 18). Thus, Foxo1 activation in lung endothelial cells plays a crucial role not only in driving alveolarization during normal lung development but also in protecting the development of the lung architecture from hyperoxia-induced damage.

5.16 The pharmacological activation of Foxo1 impacts lung structure in a mouse model of BPD

To assess whether the pharmacological activation of Foxo1 protected alveolarization from hyperoxia-induced insult, newborn wildtype mice were injected with Nab-Paclitaxel 10 µg/g or saline on P4 and P10. Nab-Paclitaxel activated Foxo1 protein expression and increased Foxo1

phosphorylation at S256 (Figure 19). No increase in the gene expression of Foxo1 was observed thus suggesting that Nab-Paclitaxel-mediated Foxo1 activation was induced through the preservation of the protein stability rather than genetical activation of Foxo1(Figure 19 and 20). The treatment with Nab-Paclitaxel induced a mild effect of protection on alveolarization by reducing the mean linear intercept by 30% (Figures 21 and 22). These data, taken together validate the causal role of the activation Foxo1 in driving lung regeneration by protecting the lung from hyperoxia-induced damage.

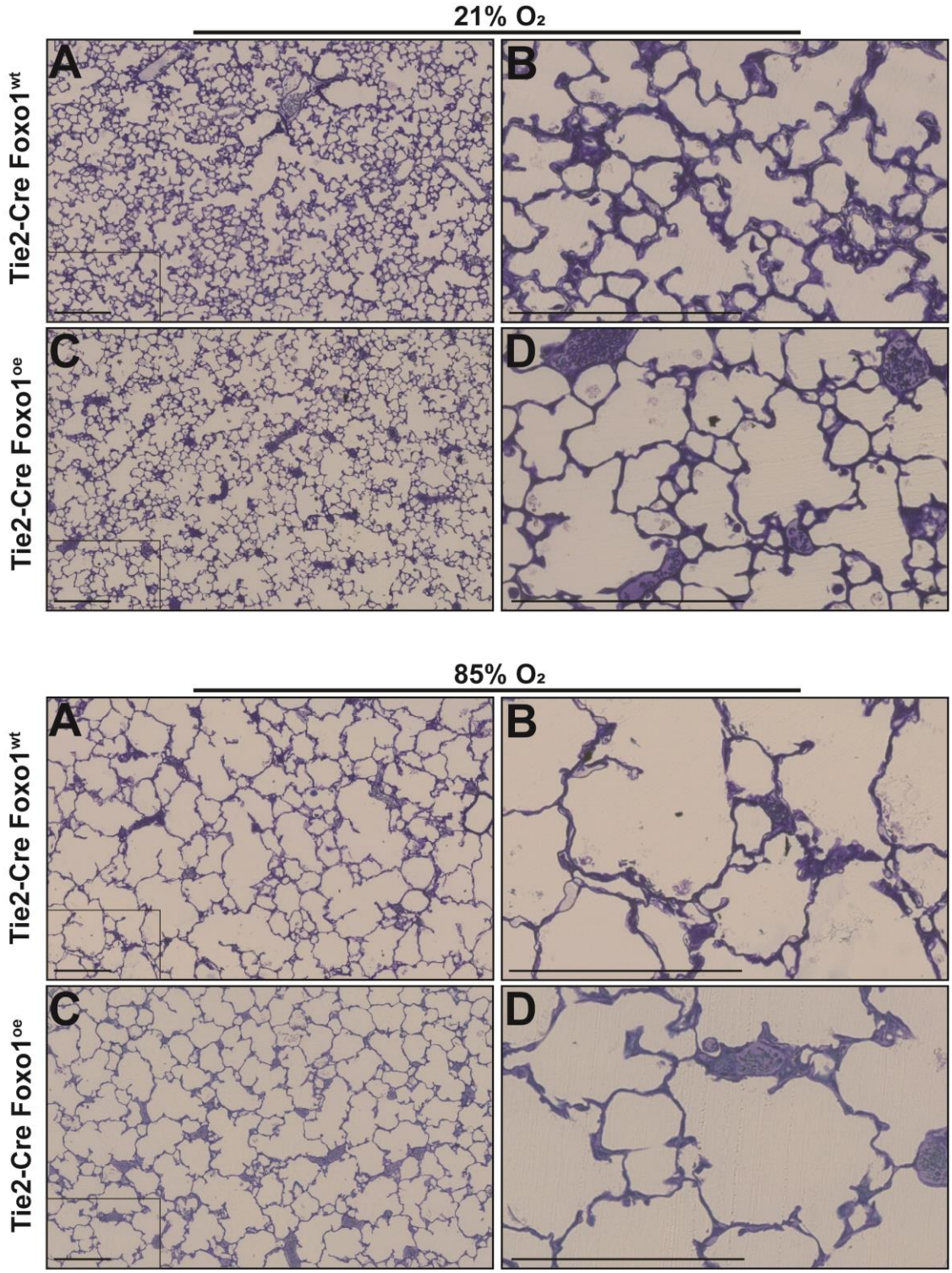

Figure 17 - Effect of the conditional upregulation of Foxo1 in lung endothelial cells on the lung structure. Representative mouse lung tissue sections from P14 Tie2-Cre Foxo1^{wt} (A,B) or Tie2-Cre Foxo1^{oe} (B,C) mice exposed to 21% or 85% O_2. wt, wildtype; oe, overexpression.

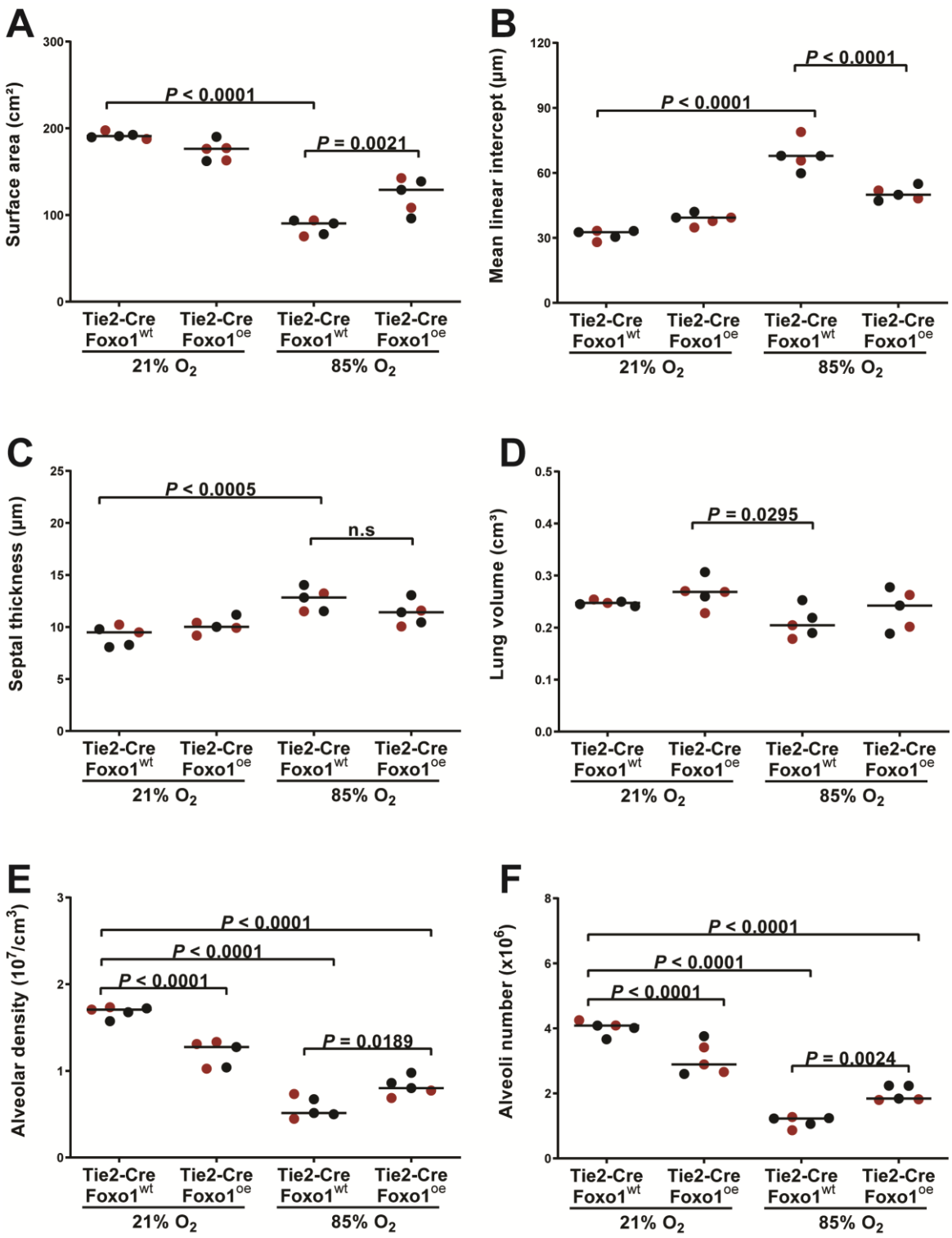

Figure 18 - Impact of the conditional upregulation of Foxo1 in lung endothelial cells on the lung structure in a mouse model of BPD. Design-based stereology was employed to assess surface area (A), mean linear intercept (B), septal thikness (C), alveolar density (E), alveoli number (F). The lung volume (D) was measured using Cavalieri method. The data represent the mean of ΔCt ± >SD. The *P* values were calculated by one-way ANOVA with Tukey's *post hoc* test. wt, wildtype; oe, overexpression, red dot, female; black dot, male

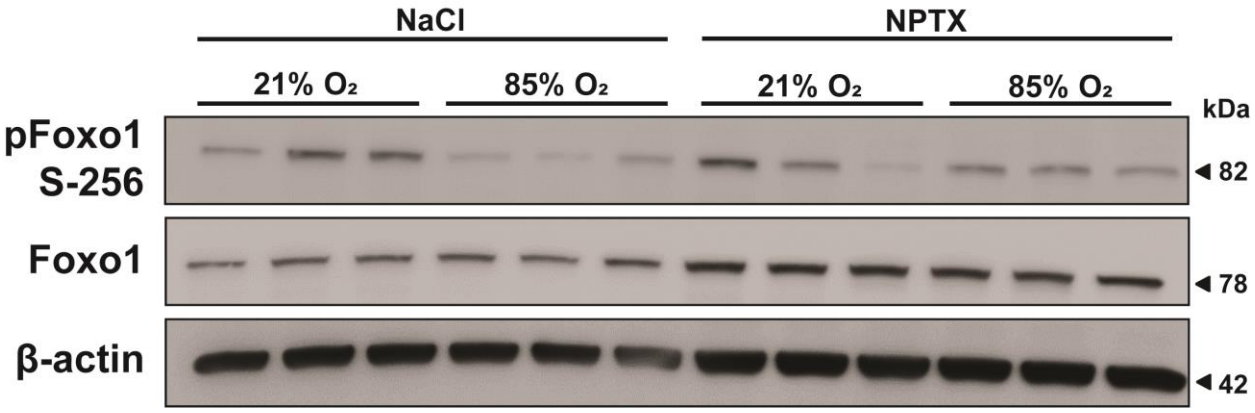

Figure 19 – Nab-Paclitaxel mediates Foxo1 activation in the postnatal lung. Representative immunoblot of Foxo1 and pFoxo1 from P14 mice exposed to 21% or 85% hyperoxia. The β-actin was used as loading control. NaCl, sodium chloride; NPTX, Nab-Paclitaxel.

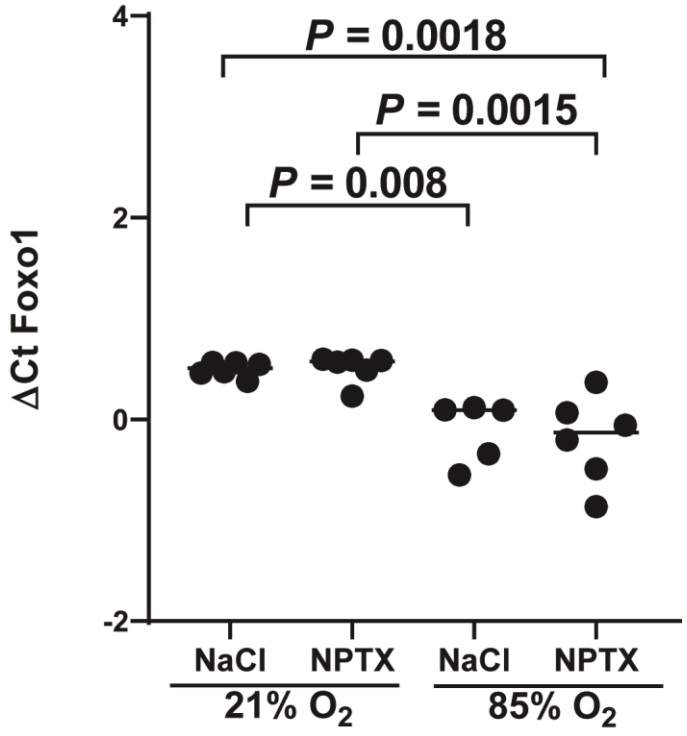

Figure 20 – Nab-Paclitaxel does not activate Foxo1 gene expression. The gene expression of Foxo1 was assessed by real-time PCR in lungs from P14 mice exposed to 21% or 85% O_2 and treated or not with Nab_Paclitaxel. The RNA polymerase gene was used as a reference. The data represent the mean of ΔCt ± SD. The *P* values were calculated by unpaired Student's *t*-test. NaCl, sodium chloride; NPTX, Nab-Paclitaxel.

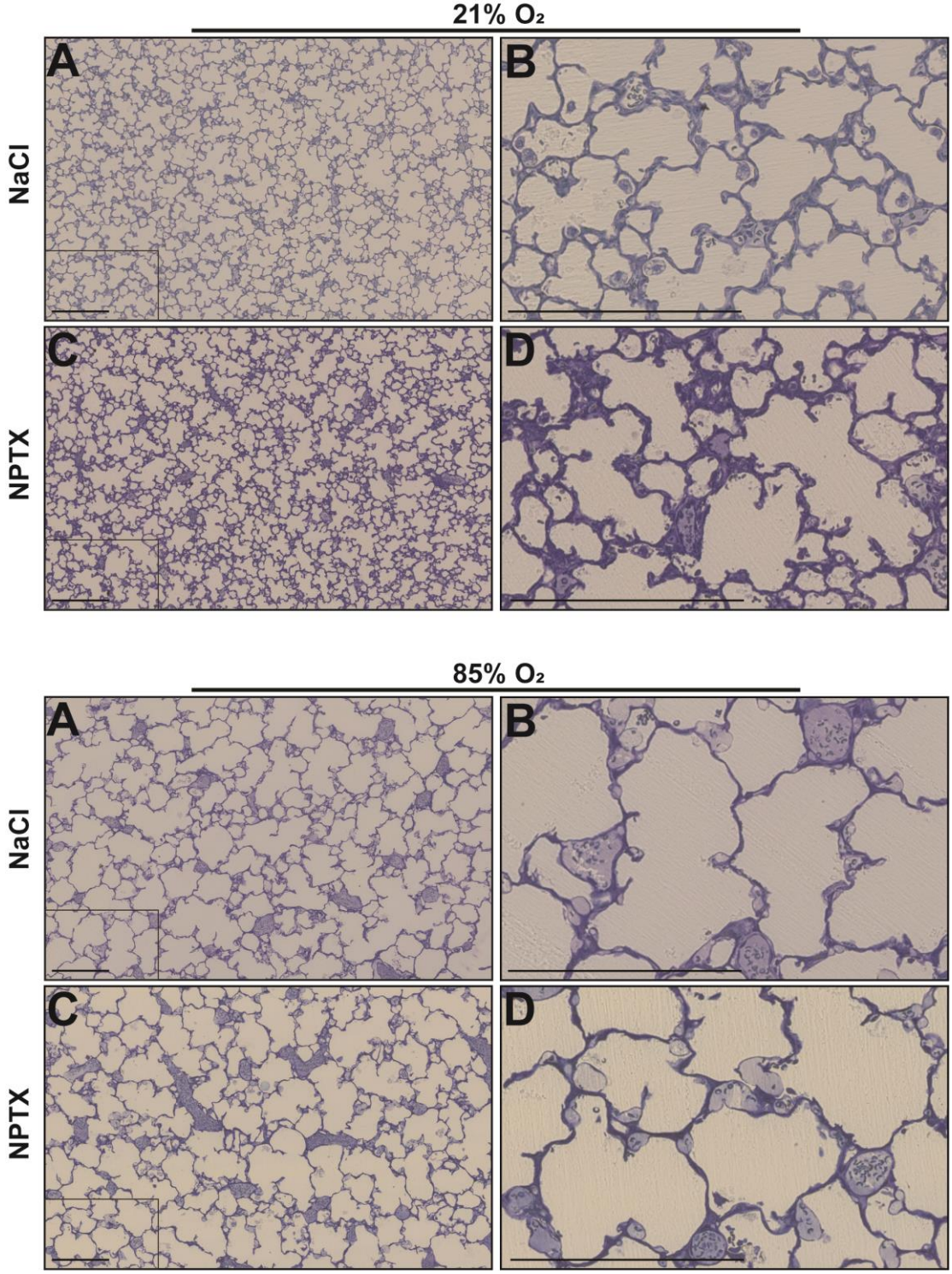

Figure 21 – Effect of the pharmacological activation of Foxo1 on the lung structure and in a mouse model of BPD. Representative mouse lung tissue sections from P14 mice injected with NaCl [A and B (A,B)] or Nab-Paclitaxel [A and B (C,D)] exposed to 21% or 85% O_2. NaCl, sodium chloride; NPTX, Nab-Paclitaxel.

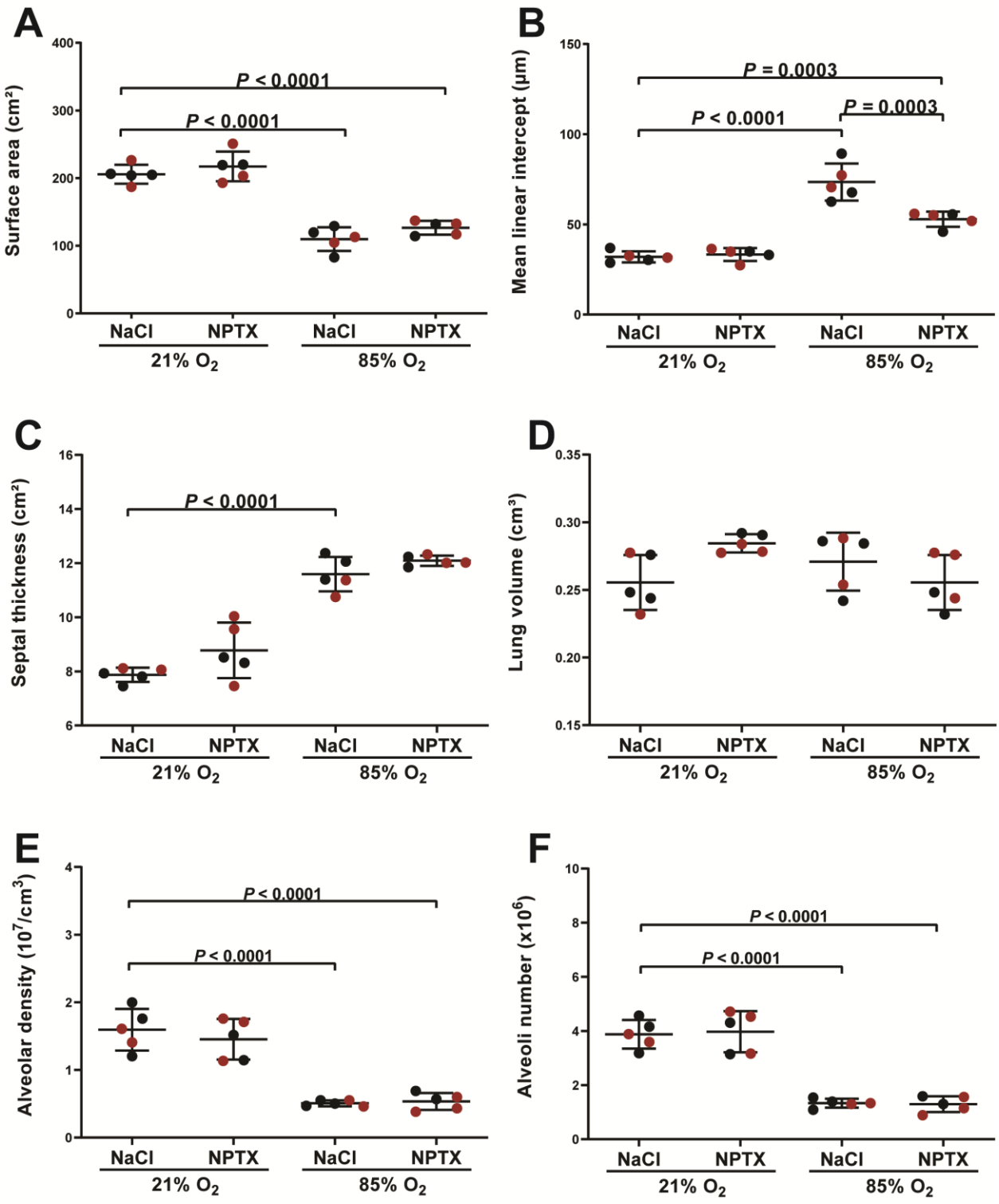

Figure 22 – Effect of Nab-Paclitaxel on the lung structure. Design-based stereology was employed to assess surface area (A), mean linear intercept (B), septal thikness (C), alveolar density (E), alveoli number (F). The lung volume (D) was measured using the Cavalieri's method. The *P* values were calculated by one-way ANOVA with Tukey's *post hoc* test. NaCl, sodium chloride; NPTX, Nab-Paclitaxel; red dot, female; black dot, male.

6 Discussion

Bronchopulmonary dysplasia is a common complication associated with preterm birth, described for the first time by Northway and collaborators (50). Preterm babies require often O_2 supplementation by mechanical ventilation. This life-saving procedure induces volume and barotrauma which together with lung infection, inflammation, pulmonary vascular remodelling and compromised respiratory function, contributes to the condition of arrested lung development known to be the hallmark of BPD (65).

The Foxo transcription factors are accreditated as crucial regulators of several developmental and pathological processes in human and mouse (9). In the context of the development of the mouse, it has been proven that Foxo1 is a pivotal regulator of vascular development (28). As such, the role of Foxo1 during the development of the lung and in response to BPD has not been elucidated. To date, this is the first study to investigate the role of the Foxo transcription factors in late lung development as well as in response to O_2 toxicity.

Foxo1 was the only transcription factor of the protein family significantly affected by hyperoxia at both mRNA and protein levels. Therefore, this study investigated gene expression and protein regulation, used flow cytometry and lung morphology to assess the role of Foxo1 in late lung development and experimental BPD.

6.1 Assessment of the Foxo transcription factors levels in late lung development and a mouse model of BPD

The Foxo transcription factors are known to regulate not only the endothelial development in the mouse (8, 23) but also the pathogenesis of several diseases (2, 63). In the context of the lung, Foxo1 is known to play an important role in lung vascular remodelling associated with PH (61). Given that the majority of preterm babies with severe BPD develop also PH, the purpose of this study was to investigate whether the Foxo transcription factors could play a role in postnatal lung development and BPD. To address the involvement of the Foxo transcription factors in the context of normal and aberrant lung development, the mRNA steady-state levels of Foxo1, Foxo3, Foxo4 and Foxo6 were analyzed in a hyperoxia-based mouse model of BPD. The employment of 85% O_2 generated mice with a lung phenotype comparable with severe BPD. In P14 mice exposed to hyperoxia, the gene expression of Foxo1 was significantly downregulated. Conversely, hyperoxia

upregulated the gene expression of Foxo3 and Foxo6. The mRNA expression of Foxo4 did not show significant changes due to hyperoxia (Figure 2) while the amount of Foxo4 protein was downregulated (Figure 4). It was not surprising that the different members of the Foxo protein family showed such a heterogeneous response. Several studies confirmed that the Foxo transcription factors, despite a high structural similarity, are capable of different regulations even in the contest of the same pathway (60). Although hyperoxia did not affect the total abundance of the protein of Foxo1, a significant downregulation of the phosphorylation of Foxo1 at S256 was observed (Figure 3A). Increased phosphorylation of Foxo1 at S256 is considered a signal of cytoplasmatic retention leading to protein degradation (14, 15). Therefore, hyperoxia increased Foxo1 nuclear sequestration. To gather a comprehensive overview of the gene expression of Foxo1 during postnatal lung development and under the effect of hyperoxia, the steady-state mRNA and protein levels of Foxo1 were analyzed on P5, P10 and P14. Hyperoxia significantly reduced the gene expression of Foxo1 only on P15 thus identifying the alveolar stage as the phase of postnatal lung development in which Foxo1 is affected by hyperoxic insult (Figure 2).

6.2 Identification of the cell types involved in the modulation of the Foxo transcription factors in experimental BPD

The ability of each cell type to express specific genes at a given time and upon specific stimuli is crucial to terminal differentiation (26). Therefore, addressing which cell types were affected by genetic perturbations of the Foxo transcription factors due to hyperoxia was of crucial interest for this study. The gene expression of Foxo1 was found higher in endothelial cells compared with the other cell types considered *in vitro* as well as from FACS-sorted lung specimens. Conversely, Foxo3 was found less expressed in lung endothelial cells compared with the other cell types analyzed. The expression of Foxo4 did not significantly vary among the cell types considered. Although Foxo6 was found significantly more expressed in pulmonary artery smooth muscle cells and microvascular endothelial cells, the expression of this gene was particularly low in every cell type considered (Figure 5). To identify in which cell types the dysregulation of the Foxo pathway was induced by hyperoxia, FACS sorting was employed to select endothelial cells, immune cells and epithelial cells from the lung of P14 mice exposed to 85% or 21% O_2. The resting cells which were not selected through specific surface markers were sorted as a “rest” population. The analysis of the gene expression by real-time PCR highlighted that Foxo1 was the only gene to be

significantly modulated due to hyperoxia (Figure 7). Those data identify Foxo1 as the only target of hyperoxia in the lung among the four Foxo genes. Furthermore, the endothelial cells are the only cell type involved in hyperoxia-induced Foxo1 downregulation.

6.3 Impact of Foxo1 expression in lung endothelial cells in experimental BPD

Several lines of evidence have shown that alterations in the gene expression of Foxo1 in mice resulted in impaired vascular development (8, 21, 28). Therefore, a crucial aim of this study was to assess whether the downregulation of Foxo1in lung endothelial cells induced by hyperoxia could be related to alterations in the structure of the lung and arrested lung development. The downregulation of Foxo1 in lung endothelial cells during postnatal lung development induced a consistent reduction in the body weight of the mice when compared with the age-matched controls (Figure 12B). Thus, suggesting arrested development. The analysis of the lung structure performed by stereological quantification showed a significant reduction in surface area, alveolar density and number. Conversely, mean linear intercept and septal thickness were significantly increased (Figures 13 and 14). On the other end, the upregulation of Foxo1 in endothelial cells protected alveolarization from hyperoxia by significantly ameliorating surface area, mean linear intercept, alveolar density and alveoli number. These data, taken together suggest that Foxo1 expression in endothelial cells is crucial not only to driving normal lung development but also in protecting lung alveolarization by hyperoxia-induced arrested lung damage. The downregulation of Foxo1 in endothelial cells is a critical signature of arrested lung development resulting in a phenotype which mirrors the condition of lung simplification induced by hyperoxia.

6.4 Analysis of the apoptosis profile of lung endothelial cells in a mouse model of BPD

The regulation of Apoptosis pathways is accreditated with a crucial role in governing several morphogenic events. During the development, apoptosis can shape organs leading to their terminal differentiation (69). For instance, it has been demonstrated that a very restricted apoptosis pattern is required to induce the digitalization of the developing limb (24). An interesting study from Kim and coworkers evaluated the involvement of apoptosis signalling in eliminating the excess of connections during the postnatal development of the brain (38). Moreover, the downregulation of apoptosis signalling is reported to play a crucial role in the vascular homeostasis of many developing organs. A reduction in the expression of the p75 neurotrophin receptor (p75ntr), an important mediator of cell apoptosis in neointimal vasculature, was shown to increase vascular

lesions in mouse carotid arteries with concomitant inflammatory cell infiltration (40). Several lines of evidence demonstrated the intimate relationship between the reduction of apoptosis signalling and vascular development *in vivo*. For instance, Tisch and coworkers proved that the postnatal deletion of Caspase 8 in endothelial cells of the mouse impaired vessel area, vascular outgrowth, number of branches and sprouting in the development of the retina (73). The conditional deletion of Caspase 8 in the mouse embryo was found to affect the development of the vasculature in the yolk sack (74). These data, taken together, demonstrate the effect of apoptotic reduction in impairing vascular development and in the context of organ pathogenesis. Furthermore, Foxo1 is accreditated with a role in the activation of apoptotic signalling (23). One of the aims of this study was to investigate the correlation between Foxo1 expression and apoptosis alterations in lung endothelial cells in normal late lung development and the context of experimental BPD. Therefore, flow cytometry and transciptomic analysis on FACS-sorted lung endothelial cells from mice exposed to hyperoxia were conducted. Hyperoxia induced a significant downregulation of the early apoptotic signalling in endothelial cells from P14 mice compared to the normoxia controls. Bulk mRNA-seq analysis from FACS-sorted endothelial cells showed that hyperoxia induced a consistent downregulation of the whole caspase signalling genes including the downstream mediator Parp1 (Figure 9). The downregulation of Foxo1 in lung endothelial cells during late lung development was able to mirror the genetic perturbations observed in hyperoxia. Foxo1 endothelial deletion decreased significantly the apoptotic signaling in P14 mice by downregulating Parp1, Cdk1a and Ccne1 (Figure 16) thus suggesting the causal role between the genetic expression of Foxo1 and early apoptosis-driven late lung development. These data highlight the role of Foxo1 as a crucial driver of alveolarization by activating early apoptotic signallings. Furthermore, Foxo1 induced early apoptosis in endothelial cells trough the activation of the extrinsic apoptosis pathway. To date, this is the first study correlating the reduction of apoptosis signaling with arrested postnatal lung development.

6.5 Pharmacological activation of Foxo1 in experimental BPD

Several lines of evidence accreditated the anti-cancer drug Nab-Paclitaxel with a role in promoting Foxo1 activation via nuclear retention, thus inducing apoptosis (61, 78, 80). Moreover, Nab-Paclitaxel Foxo1-mediated activation was able to revert vascular remodelling in a rat model of PH *in vivo* (61). Although the role of Nab-Paclitaxel as a Foxo1 activator is extensively confirmed,

the molecular mechanism of action of Nab-Paclitaxel in inducing the activation of Foxo1 is still to be elucidated. Addressing the effect of Nab-Paclitaxel as a possible treatment to protect alveolarization from hyperoxia and providing new evidence on the molecular mechanism of action of Nab-Paclitaxel was one of the aims of this study. The pharmacological activation of Foxo1 induced by administrating a low dosage (10 µg/g) of Nab-Paclitaxel at P4 and P10 in a mouse model of BPD increased the total abundance of Foxo1 protein and Foxo1 phosphorylation at S253. Notably, Nab-Paclitaxel did not increase the mRNA levels of Foxo1 (Figure 20) thus suggesting that Nab-Paclitaxel activated Foxo1 via stabilization of the protein rather than *de novo* protein production (Figure 19). To date, this is the first study providing new insight into the molecular mechanism through which Nab-Paclitaxel activates Foxo1. Furthermore, Nab-Paclitaxel-induced Foxo1 activation mildly protected the lung structure from hyperoxia by significantly ameliorating the mean linear intercept (Figures 21 and 22). These data suggest that Foxo1 pharmacological activation can be employed as a therapeutic strategy for the treatement of O_2-induced arrested lung development and accreditate Nab-Paclitaxel as a new potential intervention in the treatement BPD.

7 Abstract

Bronchopulmonary dysplasia is a common complication of the lung in premature babies characterized by decreased septation, alveolar hypoplasia, less surface area for gas exchange and dysmorphic vascular development. The Foxo transcription factors are a family of proteins accreditated with a pivotal role in the regulation of the development of the mouse and the pathogenesis of lung diseases such as cancer and pulmonary hypertension. In a hyperoxia mouse model of BPD (85% O_2), the steady-state mRNA levels of Foxo1 were significantly downregulated. The Foxo4 mRNA levels were partially reduced, Foxo3 and Foxo6 levels were upregulated. Newborn mice exposed to hyperoxia from the day of birth to the fourteenth day of life revealed a significant downregulation of the phosphorylated form of Foxo1 at S256. Hyperoxia induced protein and mRNA reduction of Foxo1 at P14. The protein expression of Foxo4 was significantly downregulated in hyperoxia. The assessment of the gene expression of the Foxo transcription factors in a cell culture-based experiment has shown a significantly higher expression of Foxo1 in lung endothelial cells compared with AT2 cells, PFBs and PASMCs. In endothelial cells FACS-sorted from the lung of P14 mice exposed to hyperoxia, Foxo1 expression was higher in endothelial cells compared to the other cell types considered. In P14 mice exposed to hyperoxia, Foxo1 mRNA levels were downregulated only in endothelial cells. Flow cytometry analysis of microvascular endothelial cells from newborn mice exposed to hyperoxia revealed a significant decrease in the apoptosis levels assessed by AnnexinV and a significant decrease in the number of endothelial cells compared with the age-matched controls. The conditional downregulation of Foxo1 gene expression in endothelial cells of newborn mice documented that the reduction of Foxo1 is crucially involved in the significant reduction of the number of endothelial cells and body mass of P14 mice. Bulk RNA-seq analysis of microvascular endothelial cells FACS-sorted from the lung of newborn mice exposed to hyperoxia showed the downregulation of genes centrally involved in the apoptotic signalling such as Parp1, Gadd45b and E2f1. The conditional downregulation of Foxo1 in lung endothelial cells of newborn mice induced the downregulation of Parp1, Ccne1 and E2f1. The assessment of the lung structure by stereological analysis showed that the conditional downregulation of Foxo1 in endothelial cells induced arrested lung development in a way comparable with the simplification of the lung structure induced by hyperoxia. The conditional upregulation of Foxo1 in the endothelial cells of newborn mice exposed to hyperoxia rescued alveolarization from hyperoxia-induced lung injury. Nab-Paclitaxel

administration of 10 µg/g on P4 and P10 activated the total amount of Foxo1 protein and the phosphorylation of Foxo1 at S256 but not the gene expression of Foxo1 in newborn wildtype mice. Stereological analysis revealed that Nab-Paclitaxel partially preserved the lung structure from hyperoxic damage. To date, this is the first study providing detailed insight into the role of Foxo1 as an important inductor of alveolarization during late lung development and a crucial modulator of the apoptotic signallings in lung endothelial cells in the contest of hyperoxia-induced lung damage. These data provide a clear picture of the function of Foxo1 not only as an important mediator of alveolarization during late lung development but also as an indispensable inducer of apoptosis in lung endothelial cells during mouse development.

8 Zusammenfassung

Bronchopulmonale Dysplasie ist eine häufige Komplikation der Lunge bei Frühgeborenen, die durch verminderte Septierung, alveoläre Hypoplasie sowie eine geringere Lungenoberfläche für den Gasaustausch und dysmorphe Gefäßentwicklung gekennzeichnet ist. Die Foxo-Transkriptionsfaktoren sind eine Familie von Proteinen, denen eine entscheidende Rolle bei der Regulierung der Entwicklung der Maus und der in der Pathogenese von Lungenkrankheiten, einschließlich Krebs und pulmonaler Hypertonie, zugeschrieben wird. Im Hyperoxie basierten BPD Model (85% O_2) die mRNA-Levels von Foxo1 signifikant herunterreguliert waren. Die Foxo4-mRNA-Levels waren teilweise reduziert, die Foxo3- und Foxo6-Levels hochreguliert waren. Neugeborene Mäuse, die vom Tag der Geburt bis zum vierzehnten Lebenstag einer Hyperoxie ausgesetzt waren, zeigten eine signifikante Verringerung der phosphorylierten Form von Foxo1 an Serin 256. Hyperoxie induzierte Protein- und mRNA-Reduktion von Foxo1 an P14. Die Proteinexpression von Foxo4 war bei Hyperoxie signifikant herunterreguliert. Die Bewertung der Genexpression der Foxo-Transkriptionsfaktoren zeigt in einem zellkulturbasierten Experiment eine signifikant höhere Expression von Foxo1 in Lungenendothelzellen im Vergleich zu AT2-Zellen, PFBs und PASMCs. In FACS-sortierten Endothelzellen aus der Lunge von P14-Mäusen, die Hyperoxie ausgesetzt waren, war die Foxo1-Expression höher in Endothelzellen im Vergleich zu allen anderen untersuchten Zelltypen. Bei P14-Mäusen, die Hyperoxie ausgesetzt waren, wurden die Foxo1-mRNA-Levels nur in Endothelzellen herunterreguliert. Die durchflusszytometrische Analyse von mikrovaskulären Endothelzellen von neugeborenen Mäusen, die Hyperoxie ausgesetzt waren, ergab eine signifikante Abnahme der durch AnnexinV bewerteten Apoptose Werte und eine signifikante Abnahme der Anzahl von Endothelzellen im Vergleich zu den altersgleichen Kontrollen. Die bedingte Herunterregulierung von Foxo1 in Endothelzellen von neugeborenen Mäusen dokumentierte, dass die Herunterregulierung von Foxo1 entscheidend an der signifikanten Verringerung der Anzahl von Endothelzellen und der Körpermasse von P14-Mäusen beteiligt war. RNA-seq von mikrovaskulären Endothelzellen, FACS-sortiert aus der Lunge neugeborener Mäuse, die Hyperoxie ausgesetzt waren, zeigte die Herunterregulierung von Genen, die zentral an der apoptotischen Signalübertragung beteiligt sind, wie Parp1, Gadd45b und E2f1. Die bedingte Herunterregulierung von Foxo1 in Lungenendothelzellen neugeborener Mäuse induzierte die Herunterregulierung von Parp1, Ccne1

und E2f1. Die Untersuchung der Lungenstruktur durch eine stereologische Analyse zeigte, dass die bedingte Herunterregulierung von Foxo1 in Endothelenzellen induzieren angehaltene Lungenentwicklungen in einer vergleichbaren Weise mit einer vereinfachten Lungenstrucktur induzierter Hyperoxie. Die bedingte Herunterregulierung der Foxo1-Genexpression in Endothelzellen neugeborener Mäuse rettet die Alveolarisation der Lunge von Schäden der Hyperoxia. Die Verabreichung von 10 µg/g Nab-Paclitaxel an P4 und P10 war in der Lage, die Gesamtmenge an Foxo1-Protein und die Phosphorylierung von Foxo1 an Serin 256 zu aktivieren, aber nicht die Genexpression von Foxo1 in neugeborenen Wildtyp-Mäusen. Die stereologische Analyse ergab, dass Nab-Paclitaxel die Lungenstruktur teilweise vor hyperoxischen Schäden bewahrte. Bis heute ist dies die erste Studie, die einen detaillierten Einblick in die Rolle von Foxo1 als wichtigen Induktor der Alveolarisierung während der späten Lungenentwicklung und als entscheidenden Modulator der apoptotischen Signalgebung in Lungenendothelzellen im Kampf gegen Hyperoxie-induzierte Lungenschäden bietet. Diese Daten liefern ein klares Bild der Funktion von Foxo1 als wichtiger Vermittler der Alveolarisation während der späten Lungenentwicklung und nicht nur als unverzichtbarer Induktor der Apoptose in Lungenendothelzellen während der Entwicklung der Maus.

9 List of Abbreviations

Ang1	angiopoietin 1
APC	allophycocyanin
AT1	alveolar type 1 pneumocytes
AT2	alveolar type 2 pneumocytes
Bak1	Bcl2 antagonist killer 1
Bax1	Bcl2 associated x regulator 1
Bcl2l1	B-cell lymphoma 2l1
BLMVECs	bovine lung microvascular endothelial cells
BPD	bronchopulmonary dysplasia
bulk RNA-seq	bulk RNA sequencing
Ccne1	Cyclin e 1
CD31	cluster of differentiation 31
CD45	cluster of differentiation 45
Cdkn1a	cyclin dependent kinase inhibitor 1a
Cdkn1b	cyclin dependent kinase inhibitor 1b
c-myc	basic helix-loop-helix transcription factor mic
Daf-16	Dauer activation faxtor 16
DAPI	4′,6-diamidino-2-phenylindole
DMEM	Dulbecco's modified eagle medium
E	embrionic
E2f1	E2f transcription factor 1
EpCam	epithelial cell adhesion molecule
FACS	fluorescent-activated cell sorting
FCS	fetal bovine serum
FELASA	federation of european laboratory animal science asociations
Flip	flice-inhibitory protein
Foxj1	forkhead box protein j1
Foxo	forkhead box o
FSC-A	forward scatter area
FSC-H	forward scatter high
Gadd45	growth arrest and DNA damage inducible protein 45
Gli2	glioma associated zinc finger protein 2
h	hour
HBSS	Hank's balanced salt solution
HEPES	4-(2-hydroxyethyl)-1-piperazineethanesulfonic acid

Hoxa10	homebox protein a10
Hoxa5	homebox protein a5
Hoxb5	homebox protein b5
HUVECs	human umbilical vein endothelial cells
Idl1	intermediate-density lipoprotein 1
Igf	insulin growth factor
Igfbp1	insulin growth factor binding protein
IP	intraperitoneal
LMECs	lung microvascular endothelial cells
mG	membrane-targeted green fluorescent protein
mT	membrane-targeted tandem dimer tomato
P1	postnatal day 1
P10	postnatal day 10
P14	postnatal day 14
P2	postnatal day 2
p21cip	cyclin-dependent kinase inhibitor 1
P30	postnatal day 30
P5	postnatal day 5
P5	postnatal day 5
P7	postnatal 7
p75ntr	p75 neurotrophin receptor
pA	polyadenylation signal
Parp1	Poly (ADP-ribose) polymerase 1
PBS	phosphate-buffered saline
Pcna	proliferating cell nuclear antigen
PCR	polymerase chain reaction
PE	phycoerythrin
Pecam1	platelet endothelial cell adhesion molecule 1
PFA	paraformaldehyde
PH	pulmonary hypertention
Pi3k	phosphoinositide 3-kinase
Pkb/Akt	protein kinase b
PVDF	polyvinylidene difluoride
qPCR	quantitative PCR
RDS	respiratory distress syndrome
real-time PCR	real-time polymerase chain reaction
RIPA	radioimmunoprecipitation assay
RNA	Ribonucleic acid
RPMI	roswell park memorial institute media
SDS	sodium dodecyl sulfate

Smad3	small mother against decapentaplegic 3
Smad4	small mother against decapentaplegic 4
SMGBM	smooth muscle cell growth basal medium
SSC-A	side scatter area
Tek	endothelial tyrosine kinase
Tgfβ	transforming growth factorβ
VEGF	vascular endothelial growth factor
VPCs	vascular proliferating endothelial cells
Wk	week

10 List of Figures

11 List of Tables

12 Bibliography

1. Accili D, Arden KC. FoxOs at the crossroads of cellular metabolism, differentiation, and transformation. Cell. 2004; 117(4):421-6.

2. Al-Tamari HM, Dabral S, Schmall A, Sarvari P, Ruppert C, Paik J, DePinho RA, Grimminger F, Eickelberg O, Guenther A, Seeger W, Savai R, Pullamsetti SS. FoxO3 an important player in fibrogenesis and therapeutic target for idiopathic pulmonary fibrosis. EMBO Mol Med. 2018; 10(2):276-293.

3. Al Alam D, El Agha E, Sakurai R, Kheirollahi V, Moiseenko A, Danopoulos S, Shrestha A, Schmoldt C, Quantius J, Herold S, Chao CM, Tiozzo C, De Langhe S, Plikus M V., Thornton M, Grubbs B, Minoo P, Rehan VK, Bellusci S. Evidence for the involvement of fibroblast growth factor 10 in lipofibroblast formation during embryonic lung development. Development. 2015; 142(23):4139-50.

4. Albertine KH. Utility of large-animal models of BPD: chronically ventilated preterm lambs. Am J Physiol Lung Cell Mol Physiol. 2015; 308(10):L983-L1001.

5. Almeida M, Han L, Martin-Millan M, O'Brien CA, Manolagas SC. Oxidative stress antagonizes Wnt signaling in osteoblast precursors by diverting β-catenin from T cell factor to forkhead box O-mediated transcription. J Biol Chem. 2007; 282(37):27298-27305.

6. Alvira CM. Aberrant pulmonary vascular growth and remodeling in bronchopulmonary dysplasia. Front. Med. 2016; 3:21.

7. Ambalavanan N, Morty RE. Searching for better animal models of BPD: A perspective. Am J Physiol Lung Cell Mol Physiol. 2016; 311(5):L924-L927.

8. Andrade J, Shi C, Costa ASH, Choi J, Kim J, Doddaballapur A, Sugino T, Ong YT, Castro M, Zimmermann B, Kaulich M, Guenther S, Wilhelm K, Kubota Y, Braun T, Koh GY, Grosso AR, Frezza C, Potente M. Control of endothelial quiescence by FOXO-regulated metabolites. Nat Cell Biol. 2021; 23(4):413-423.

9. Arden KC. FOXO animal models reveal a variety of diverse roles for FOXO transcription factors. Oncogene. 2008; 27(16):2345-50.

10. Aubin J, Lemieux M, Tremblay M, Bérard J, Jeannotte L. Early postnatal lethality in Hoxa-5 mutant mice is attributable to respiratory tract defects. Dev Biol. 1997; 192(2):432-45.

11. Barkauskas CE, Cronce MJ, Rackley CR, Bowie EJ, Keene DR, Stripp BR, Randell SH, Noble PW, Hogan BLM. Type 2 alveolar cells are stem cells in adult lung. J Clin Invest. 2013; 123(7):3025-36.

12. Berger J, Bhandari V. Animal models of bronchopulmonary dysplasia. The term mouse models. Am J Physiol Lung Cell Mol Physiol. 2014; 307(12):L936-47.

13. Biggs WH, Cavenee WK, Arden KC. Identification and characterization of members of the

FKHR (FOX O) subclass of winged-helix transcription factors in the mouse. Mamm Genome. 2001; 12(6):416-25.

14. Biggs WH, Meisenhelder J, Hunter T, Cavenee WK, Arden KC. Protein kinase B/Akt-mediated phosphorylation promotes nuclear exclusion of the winged helix transcription factor FKHR1. Proc Natl Acad Sci U S A. 1999; 96(13):7421-6.

15. Brunet A, Bonni A, Zigmond MJ, Lin MZ, Juo P, Hu LS, Anderson MJ, Arden KC, Blenis J, Greenberg ME. Akt promotes cell survival by phosphorylating and inhibiting a forkhead transcription factor. Cell. 1999; 96(6):857-68.

16. Cardoso W V. Molecular regulation of lung development. Annu. Rev. Physiol. 2001; 63:471-94.

17. Chao CM, El Agha E, Tiozzo C, Minoo P, Bellusci S. A breath of fresh air on the mesenchyme: Impact of impaired mesenchymal development on the pathogenesis of bronchopulmonary dysplasia. Front. Med. 2015; 2:27.

18. Chen J, Knowles HJ, Hebert JL, Hackett BP. Mutation of the mouse hepatocyte nuclear factor/forkhead homologue 4 gene results in an absence of cilia and random left-right asymmetry. J Clin Invest. 1998; 102(6):1077-82.

19. Collins JJP, Tibboel D, de Kleer IM, Reiss IKM, Rottier RJ. The future of bronchopulmonary dysplasia: Emerging pathophysiological concepts and potential new avenues of treatment. Front Med. 2017; 4:61.

20. D'Angio CT, Ryan RM. Animal models of bronchopulmonary dysplasia. The preterm and term rabbit models. Am J Physiol Lung Cell Mol Physiol. 2014; 307(12):L959-69.

21. Daly C, Wong V, Burova E, Wei Y, Zabski S, Griffiths J, Lai KM, Lin HC, Ioffe E, Yancopoulos GD, Rudge JS. Angiopoietin-1 modulates endothelial cell function and gene expression via the transcription factor FKHR (FOXO1). Genes Dev. 2004; 18(9):1060-71.

22. De Paepe ME, Mao Q, Powell J, Rubin SE, DeKoninck P, Appel N, Dixon M, Gundogan F. Growth of pulmonary microvasculature in ventilated preterm infants. Am J Respir Crit Care Med. 2006; 173(2):204-11.

23. Dharaneeswaran H, Abid MR, Yuan L, Dupuis D, Beeler D, Spokes KC, Janes L, Sciuto T, Kang PM, Jaminet SCS, Dvorak A, Grant MA, Regan ER, Aird WC. FoxO1-Mediated Activation of Akt Plays a Critical Role in Vascular Homeostasis. Circ Res. 2014; 115(2):238-251.

24. Farin HF, Lüdtke THW, Schmidt MK, Placzko S, Schuster-Gossler K, Petry M, Christoffels VM, Kispert A. Tbx2 Terminates Shh/Fgf Signaling in the Developing Mouse Limb Bud by Direct Repression of Gremlin1. PLoS Genet. 2013; 9(4):e1003467.

25. Fehl J, Pozarska A, Nardiello C, Rath P, Surate Solaligue DE, Vadász I, Mayer K, Herold S, Seeger W, Morty RE. Control interventions can impact alveolarization and the transcriptome in developing mouse lungs. Anat Rec. 2019; 302(2):346-363.

26. Florio M, Heide M, Pinson A, Brandl H, Albert M, Winkler S, Wimberger P, Huttner WB, Hiller M. Evolution and cell-type specificity of human-specific genes preferentially expressed in progenitors of fetal neocortex. Elife. 2018; 7:e32332.

27. Fu Z, Tindall DJ. FOXOs, cancer and regulation of apoptosis. Oncogene. 2008; 27(16):2312-9.

28. Furuyama T, Kitayama K, Shimoda Y, Ogawa M, Sone K, Yoshida-Araki K, Hisatsune H, Nishikawa SI, Nakayama K, Nakayama K, Ikeda K, Motoyama N, Mori N. Abnormal angiogenesis in Foxo1 (Fkhr)-deficient mice. J Biol Chem. 2004; 279(33):34741-9.

29. Geetha O, Rajadurai VS, Anand AJ, Dela Puerta R, Huey Quek B, Khoo PC, Chua MC, Agarwal P. New BPD-prevalence and risk factors for bronchopulmonary dysplasia/mortality in extremely low gestational age infants ≤28 weeks. J Perinatol. 2021; 41(8):1943-1950.

30. Greer EL, Brunet A. FOXO transcription factors at the interface between longevity and tumor suppression. Oncogene. 2005. Oncogene; 24(50):7410-25.

31. Haies DM, Gil J, Weibel ER. Morphometric study of rat lung cells. I. Numerical and dimensional characteristics of parenchymal cell population. Am Rev Respir Dis. 1981; 123(5):533-41.

32. Hosaka T, Biggs WH, Tieu D, Boyer AD, Varki NM, Cavenee WK, Arden KC. Disruption of forkhead transcription factor (FOXO) family members in mice reveals their functional diversification. Proc Natl Acad Sci U S A. 2004; 101(9):2975-80.

33. Hsia CCW, Hyde DM, Ochs M, Weibel ER. An official research policy statement of the American Thoracic Society/European Respiratory Society: Standards for quantitative assessment of lung structure. Am J Respir Crit Care Med. 2010; 181(4):394-418.

34. Keller C, Arenkiel BR, Coffin CM, El-Bardeesy N, DePinho RA, Capecchi MR. Alveolar rhabdomyosarcomas in conditional Pax3:Fkhr mice: Cooperativity of Ink4a/ARF and Trp53 loss of function. Genes Dev. 2004; 18(21):2614-26.

35. Kim HY, Pang MF, Varner VD, Kojima L, Miller E, Radisky DC, Nelson CM. Localized Smooth Muscle Differentiation Is Essential for Epithelial Bifurcation during Branching Morphogenesis of the Mammalian Lung. Dev Cell. 2015; 34(6):719-26.

36. Kim JJ, Taylor HS, Akbas GE, Foucher I, Trembleau A, Jaffe RC, Fazleabas AT, Unterman TG. Regulation of insulin-like growth factor binding protein-1 promoter activity by FKHR and HOXA10 in primate endometrial cells. Biol Reprod. 2003; 68(1):24-30.

37. Kim WR, Sun W. Programmed cell death during postnatal development of the rodent nervous system. Dev Growth Differ. 2011; 53(2):225-35.

38. Korhonen H, Fisslthaler B, Moers A, Wirth A, Habermehl D, Wieland T, Schütz G, Wettschureck N, Fleming I, Offermanns S. Anaphylactic shock depends on endothelial Gq/G11. J Exp Med. 2009; 206(2):411-20.

39. Kraemer R. Reduced apoptosis and increased lesion development in the flow-restricted carotid artery of p75NTR-null mutant mice. Circ Res. 2002; 91(6):494-500.

40. Kramer BW. Antenatal inflammation and lung injury: Prenatal origin of neonatal disease. J Perinatol. 2008; 1:S21-7.

41. Lin K, Dorman JB, Rodan A, Kenyon C. daf-16: An HNF-3/forkhead family member that can function to double the life-span of Caenorhabditis elegans. Science. 1997; 278(5341):1319-22.

42. Matsukawa M, Sakamoto H, Kawasuji M, Furuyama T, Ogawa M. Different roles of Foxo1 and Foxo3 in the control of endothelial cell morphology. Genes Cells. 2009; 14(10):1167-81.

43. Moiseenko A, Kheirollahi V, Chao CM, Ahmadvand N, Quantius J, Wilhelm J, Herold S, Ahlbrecht K, Morty RE, Rizvanov AA, Minoo P, El Agha E, Bellusci S. Origin and characterization of alpha smooth muscle actin-positive cells during murine lung development. Stem Cells. 2017; 35(6):1566-1578.

44. Motoyama J, Liu J, Mo R, Ding Q, Post M, Hui CC. Essential function of Gli2 and Gli3 in the formation of lung, trachea and oesophagus. Nat Genet. 1998; 20(1):54-7.

45. Mourani PM, Sontag MK, Younoszai A, Miller JI, Kinsella JP, Baker CD, Poindexter BB, Ingram DA, Abman SH. Early pulmonary vascular disease in preterm infants at risk for bronchopulmonary dysplasia. Am J Respir Crit Care Med. 2015; 191(1):87-95.

46. Muzumdar MD, Tasic B, Miyamichi K, Li N, Luo L. A global double-fluorescent cre reporter mouse. Genesis. 2007; 45(9):593-605.

47. Najaf T, Hebert JL, Hackett BP. Defect in Pulmonary Ciliogenesis in Mice with a Targeted Mutation in the Hepatocyte Nuclear Factor/Forkhead Homologue 4 Gene. Pediatr Res. 1999; 0031-3998.

48. Nardiello C, Mižková I, Silva DM, Ruiz-Camp J, Mayer K, Vadász I, Herold S, Seeger W, Morty RE. Standardisation of oxygen exposure in the development of mouse models for bronchopulmonary dysplasia. Dis Model Mech. 2017; 10(2):185-196.

49. Northway WH, Rosan RC, Porter DY. Pulmonary disease following respirator therapy of hyaline-membrane disease. Bronchopulmonary dysplasia. N Engl J Med. 1967; 276(7):357-68.

50. O'Reilly M, Thébaud B. Animal models of bronchopulmonary dysplasia. The term rat models. Am J Physiol Lung Cell Mol Physiol. 2014; 307(12):L948-58.

51. Oli V, Gupta R, Kumar P. FOXO and related transcription factors binding elements in the regulation of neurodegenerative disorders. J Chem Neuroanat. 2021; 116:102012.

52. Ouyang W, Liao W, Luo CT, Yin N, Huse M, Kim M V., Peng M, Chan P, Ma Q, Mo Y, Meijer D, Zhao K, Rudensky AY, Atwal G, Zhang MQ, Li MO. Novel Foxo1-dependent transcriptional programs control T reg cell function. Nature. 2012; 491(7425):554-9.

53. Polter A, Yang S, Zmijewska AA, van Groen T, Paik JH, DePinho RA, Peng SL, Jope RS, Li X. Forkhead box, class O transcription factors in brain: regulation and behavioral manifestation. Biol Psychiatry. 2009; 65(2):150-9.

54. Potente M, Urbich C, Sasaki KI, Hofmann WK, Heeschen C, Aicher A, Kollipara R, DePinho RA, Zeiher AM, Dimmeler S. Involvement of Foxo transcription factors in angiogenesis and postnatal neovascularization. J Clin Invest. 2005; 115(9):2382-92.

55. Rath P, Nardiello C, Surate Solaligue DE, Agius R, Mižíková I, Hühn S, Mayer K, Vadász I, Herold S, Runkel F, Seeger W, Morty RE. Caffeine administration modulates TGF-β signaling but does not attenuate blunted alveolarization in a hyperoxia-based mouse model of bronchopulmonary dysplasia. Pediatr Res. 2017; 81(5):795-805.

56. Rock JR, Barkauskas CE, Cronce MJ, Xue Y, Harris JR, Liang J, Noble PW, Hogan BLM. Multiple stromal populations contribute to pulmonary fibrosis without evidence for epithelial to mesenchymal transition. Proc Natl Acad Sci U S A. 2011; 108(52):E1475-83.

57. Ronnebaum SM, Patterson C. The FoxO Family in Cardiac Function and Dysfunction. Annu Rev Physiol. 2010; 72:81-94.

58. Ruiz-Camp J, Quantius J, Lignelli E, Arndt PF, Palumbo F, Nardiello C, Surate Solaligue DE, Sakkas E, Mižíková I, Rodríguez-Castillo JA, Vadász I, Richardson WD, Ahlbrecht K, Herold S, Seeger W, Morty RE. Targeting miR-34a/ Pdgfra interactions partially corrects alveologenesis in experimental bronchopulmonary dysplasia . EMBO Mol Med. 2019; 11(3):e9448.

59. Sanchez AMJ, Candau RB, Bernardi H. FoxO transcription factors: Their roles in the maintenance of skeletal muscle homeostasis. Cell Mol Life Sci. 2014; 71(9):1657-71.

60. Savai R, Al-Tamari HM, Sedding D, Kojonazarov B, Muecke C, Teske R, Capecchi MR, Weissmann N, Grimminger F, Seeger W, Schermuly RT, Savai PS. Pro-proliferative and inflammatory signaling converge on FoxO1 transcription factor in pulmonary hypertension. Nat Med. 2014; 20(11):1289-300.

61. Scherle W. A simple method for volumetry of organs in quantitative stereology. Mikroskopie. 1970; 26(1):57-60.

62. Sengupta A, Molkentin JD, Paik JH, DePinho RA, Yutzey KE. FoxO transcription factors promote cardiomyocyte survival upon induction of oxidative stress. J Biol Chem. 2011; 286(9):7468-78.

63. Seoane J, Le H Van, Shen L, Anderson SA, Massagué J. Integration of Smad and forkhead pathways in the control of neuroepithelial and glioblastoma cell proliferation. Cell. 2004; 117(2):211-23.

64. Silva DMG, Nardiello C, Pozarska A, Morty RE. Recent advances in the mechanisms of lung alveolarization and the pathogenesis of bronchopulmonary dysplasia. Am J Physiol Lung Cell Mol Physiol. 2015; 309(11):L1239-72.

65. Sinkin RA, Phelps DL. New strategies for the prevention of bronchopulmonary dysplasia.

Clin Perinatol. 1987; 14(3):599-620.

66. Skurk C, Maatz H, Kim HS, Yang J, Abid R, Aird WC, Walsh K. The Akt-regulated forkhead transcription factor FOXO3a controls endothelial cell viability through modulation of the Caspase-8 inhibitor FLIP. J Biol Chem. 2004; 279(2):1513-25.

67. Stone KC, Mercer RR, Gehr P, Stockstill B, Crapo JD. Allometric relationships of cell numbers and size in the mammalian lung. Am J Respir Cell Mol Biol. 1992; 6(2):235-43.

68. Suzanne M, Steller H. Shaping organisms with apoptosis. Cell Death Differ. 2013; 20(5):669-75.

69. Thébaud B, Abman SH. Bronchopulmonary dysplasia: Where have all the vessels gone? Roles of angiogenic growth factors in chronic lung disease. Am J Respir Crit Care Med. 2007; 175(10):978-85.

70. Tikhanovich I, Cox J, Weinman SA. FOXO Transcription Factors in Liver Function and Disease. J Gastroenterol Hepatol. 2013; 28(1):125-131.

71. Tiono J, Surate Solaligue DE, Mižíková I, Nardiello C, Vadász I, Böttcher-Friebertshäuser E, Ehrhardt H, Herold S, Seeger W, Morty RE. Mouse genetic background impacts susceptibility to hyperoxia-driven perturbations to lung maturation. Pediatr Pulmonol. 2019; 54(7):1060-1077.

72. Tisch N, Freire-Valls A, Yerbes R, Paredes I, Porta S La, Wang X, Martín-Pérez R, Castro L, Wong WWL, Coultas L, Strilic B, Gröne HJ, Hielscher T, Mogler C, Adams RH, Heiduschka P, Claesson-Welsh L, Mazzone M, López-Rivas A, Schmidt T, Augustin HG, De Almodovar CR. Caspase-8 modulates physiological and pathological angiogenesis during retina development. J Clin Invest. 2019; 129(12):5092-5107.

73. Tisch N, Ruiz de Almodóvar C. Contribution of cell death signaling to blood vessel formation. Cell Mol Life Sci. 2021; 78(7):3247-3264.

74. Tsuji-Tamura K, Ogawa M. Inhibition of the PI3K-Akt and mTORC1 signaling pathways promotes the elongation of vascular endothelial cells. J Cell Sci. 2016; 129(6):1165-78.

75. Van Der Vos KE, Coffer PJ. FOXO-binding partners: it takes two to tango. Oncogene. 2008; 27(16):2289-99.

76. Varghese N, Rios D. Pulmonary Hypertension Associated with Bronchopulmonary Dysplasia: A Review. Pediatr Allergy Immunol Pulmonol. 2019; 32(4):140-148.

77. Wang J, Yang H, Li W, Xu H, Yang X, Gan L. Thioredoxin 1 upregulates FOXO1 transcriptional activity in drug resistance in ovarian cancer cells. Biochim Biophys Acta. 2015; 1852(3):395-405.

78. Weismann CG, Asnes JD, Bazzy-Asaad A, Tolomeo C, Ehrenkranz RA, Bizzarro MJ. Pulmonary hypertension in preterm infants: Results of a prospective screening program. J Perinatol. 2017; 37(5):572-577.

79. Xu K, Zhu W, Xu A, Xiong Z, Zou D, Zhao H, Jiao D, Qing Y, Jamal MA, Wei HJ, Zhao HY. Inhibition of FOXO1-mediated autophagy promotes paclitaxel-induced apoptosis of MDA-MB-231 cells. Mol Med Rep. 2022; 25(2):72.

80. Yoder BA, Coalson JJ. Animal models of bronchopulmonary dysplasia. The preterm baboon models. Am J Physiol Lung Cell Mol Physiol. 2014; 307(12)

13 Declaration

I declare that I have completed this dissertation single-handedly without the unauthorized help of a second party and only with the assistance acknowledged therein. I have appropriately acknowledged and referenced all text passages that are derived literally from or are based on the content of published or unpublished work of others, and all information that relates to verbal communications. I have abided by the principles of good scientific conduct laid down in the charter of the Justus Liebig University of Giessen in carrying out the investigations described in the dissertation.